Ann. Rev. Astron. Astrophys. 1980. 18 : 489–535

MEASUREMENTS OF THE COSMIC BACKGROUND RADIATION

Rainer Weiss[1]
Department of Physics, Massachusetts Institute of Technology,
Cambridge, Massachusetts 02139

INTRODUCTION

This article presents a critical review of measurements of the attributes of the cosmic background radiation and indicates the prospects for improved measurements. Since the last review in these volumes (Thaddeus 1972), there has been substantial progress in the field and of course several other review articles (Alpher & Herman 1975, Danese & DeZotti 1977, Ulfbeck 1980). An up-to-date review of theoretical work on the background is presented by Sunyaev & Zel'dovich (1980) in this volume.

Whether one's taste runs to the presently favored "big bang" cosmology or to more heretical models, the background radiation has become an accepted and essential part of observational cosmology. The radiation has unique and remarkable properties: it is isotropic on both large and small angular scales to a higher degree than any other source in the universe; it exhibits no linear polarization; and it has a spectrum so close to that of a blackbody that one can talk only of deviations from a thermal spectrum. In short, the radiation satisfies beyond almost reasonable expectations the simple hypothesis that it is a remnant of a homogeneous and structureless primeval explosion. The observed blandness and apparent pristine state of the radiation beg for more detail. One hopes that precision observations would show imprints left by early cosmic processes and that observed deviations could be fruitfully interpreted. Studies of the background radiation have passed the discovery phase and are beginning an analytic one.

This review is dedicated to the analytic phase. How well have the

[1] Supported in part by NASA Grant NGR 22-009-526.

0066-4146/80/0915-0489$01.00

spectrum, intensity distribution on large angular scales, and polarization been measured? What limits these measurements and where is there a reasonable chance for improvement?

MEASUREMENTS OF THE SPECTRUM

Absolute measurements are always difficult. Measurements of the cosmic background radiation (CBR) spectrum are no exception and are further complicated by the fact that it is impossible to modulate the signal, the CBR. The CBR is therefore the residue, what is left over after one has accounted for everything else. The quality of this accounting, the precision and reliability of measurement of the individual terms, determines the value of the observation. The evolution of experiments to measure the CBR spectrum demonstrates this well. Future progress lies in improved experimental design or operation in more benign environments which permit reduction of the most uncertain elements in the accounting sum.

Direct measurements of the CBR spectrum fall crudely into two categories: low frequency observations in the Rayleigh-Jeans portion of the spectrum and observations at high frequencies in the region embracing the blackbody peak and into the Wien tail. This categorization results from the different technologies used in the two regions, and differences between the magnitudes of the terrestrial atmospheric emission. The low frequency measurements employ conventional microwave technology—coherent receivers—at sea-level and mountain observing sites while the high frequency observations have been carried out with less well developed infrared techniques—incoherent detectors, broad-band filters, Fourier transform spectrometers—on balloon- and rocket-borne platforms.

As the sub-millimeter technology of coherent receivers, in particular the development of efficient broad-band mixers, improves, the low frequency techniques will be applied to the high frequency region from balloon and aircraft platforms.

Figure 1 outlines the basis of all the low frequency measurements. The individual experiments listed in Table 1 may differ in details, even in some important ones, but nevertheless all consist of the same components: a

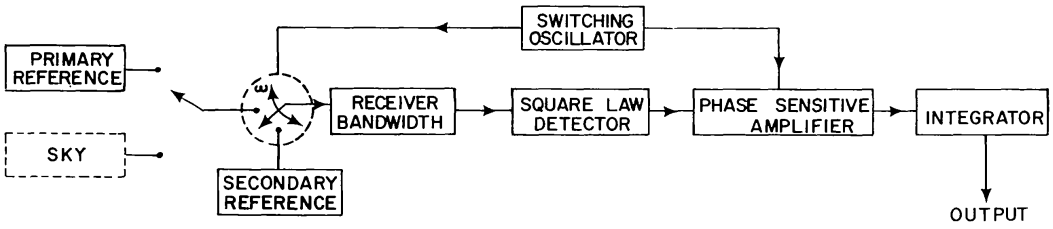

Figure 1 Schematic diagram of a generic absolute radiometer.

coherent receiver, a primary absolute reference calibrator, and an antenna The experimental strategy has been to compare the radiation entering the antenna with that of the primary calibrator, the gain of the receiver being determined by either varying the temperature of the primary reference or by injecting a known power into the receiver input.

(*a*) *Receivers*

The receiver sensitivity is often specified in terms of the smallest measurable change in temperature of a Rayleigh-Jeans thermal source that covers the entire antenna aperture, in a post-detection bandwidth of 1 Hz—an integration time of approximately 1/2 second. The minimum detectable temperature change is given by

$$T_{\min}(\mathrm{K/Hz^{1/2}}) = gT_{\mathrm{system}}/B^{1/2} \tag{1}$$

where g is a factor between 1 and 2 determined by the type of modulation and integrating filter. B is the receiver bandwidth determined by the mixer or the intermediate frequency amplifier. The system noise is characterized by T_{system}, the temperature of a fictitious Rayleigh-Jeans source placed over the antenna aperture that would produce the same *fluctuations* in a noise-free receiver output as are actually observed.

The early experiments had system temperatures of several thousand degrees and receiver bandwidths of tens of MHz, which permitted measurements to 1/10 degree in an integration time of about 1 minute. Inadequate receiver sensitivity has never been a real limit in these measurements except in the process of measuring some of the systematic noise sources, in particular the contribution from antenna side lobes, and in some of the experiments, the atmospheric radiation. The reasons for this will become clearer when each of these terms is discussed below.

The system output signal is proportional to the integral of the input power spectral density over the receiver bandwidth. The receivers, however, amplify the currents and voltages at the input terminals which are proportional to the incident electric and magnetic fields and are therefore sensitive to the phases of these fields. The receiver and antenna together are generally designed to accept one spatial mode (and often one polarization state) of the radiation field. For coherent systems like this the area—solid angle product (étendue) is λ^2. The total power accepted from an isotropic blackbody distribution is then

$$\Delta P = \frac{hf}{e^{hf/kT}-1}\,B, \qquad f \gg B. \tag{2}$$

The receiver systems are usually calibrated with blackbody sources for which $hf/kT \ll 1$ (Rayleigh-Jeans sources). For example at $\lambda = 1$ cm, $T = 300$ K, $hf/kT \sim 5\times 10^{-3}$ so that the receiver power is just equal to

Table 1 Heterodyne measurements of the cosmic background spectrum

Reference	λ (cm)	f (GHz)	ν (cm^{-1})	Altitude (km)	Receiver noise ($K/Hz^{1/2}$)	Beam width (deg.)	Properties of primary calibrator: Thermodynamic temperature of primary ref.	Antenna temperature of primary ref.	$\varepsilon_p T_p$ (K)	R	$\varepsilon_w T_w$ (K)
Howell & Shakeshaft 1967	73.5	0.41	0.014	0	—	15	4.2	4.19	1.7 ± 0.2	—	—
	49.2	0.61	0.020						1.4 ± 0.2		
Penzias & Wilson 1967	21.2	1.415	0.047	0	—	—	4.2	4.17	0.6	—	—
Howell & Shakeshaft 1966	20.7	1.41	0.048	0	—	13×15	4.2	4.17	1.7 ± 0.2	—	—
Penzias & Wilson 1965, Penzias 1968	7.35	4.08	0.136	0	—	—	4.2	4.10	1.3	—	—
Roll & Wilkinson 1966	3.2	9.37	0.313	0	—	20	4.2	3.98	2.6 ± 0.35	—	—
Stokes et al. 1967	3.2	9.37	0.313	3.8	~1.5	4	3.77	3.55	0.16 ± 0.10	$6 \pm 3 \times 10^{-4}$	0.06 ± 0.02
Stokes et al. 1967	1.58	19.0	0.633	3.8	~1.5	4	3.77	3.33	0.21 ± 0.08	$1 \pm 0.3 \times 10^{-3}$	0.04 ± 0.01
Welch et al. 1967	1.5	20.0	0.666	3.8	~2	12	73.6	73.12	0.42 ± 0.1	$<4.10^{-4}$	—
Ewing et al. 1967	0.924	32.5	1.08	3.8	~3	20	3.78	3.056	1.0 ± 0.15	—	0.06 ± 0.02
Wilkinson 1967	0.856	35.05	1.168	3.8	~1.5	4	3.77	2.99	0.28 ± 0.11	$0 \pm 3 \times 10^{-4}$	0.06 ± 0.06
Puzanov et al. 1968	0.82	36.6	1.22	0	1.6	4	77.36	76.48	—	—	—
Kislyakov et al. 1971	0.358	83.8	2.79	3	2–4	10	~75.0	~73.0	—	—	—
Boynton et al. 1968	0.33	90.0	3.00	3.44	1.5	—	3.8	2.042	0.22 ± 0.11	3×10^{-4}	0.27 ± 0.04
Millea et al. 1971	0.33	90.4	3.00	3.1	0.5	6.6	3.85	2.087	1.1 ± 0.11	$3 \pm 0.6 \times 10^{-4}$	—
				2.8			3.88	2.114			
Boynton & Stokes 1974	0.33	90.0	3.00	14.9	0.1	—	4.2	2.405	0.22 ± 0.11	$8 \pm 4 \times 10^{-4}$	0.27 ± 0.04

Table 1—*continued*

Reference	Properties of antenna		External sources[a]		Switch asymmetry	Cosmic background thermodynamic temperature	See note[b]
	$\varepsilon_{ant} T_{ant}$ (K)	$f\varepsilon_{gnd} T_{gnd}$ (K)	$\varepsilon_{atm} T_{atm}$ (K)	T_{gal} (K)			
Howell & Shakeshaft 1967	0.4±0.2 0.4±0.2	0.6±0.4 0.6±0.4	1.3±0.1 1.95±0.1	20.6±2.2 6.7±0.7	—	3.7±1.2	1, 2
Penzias & Wilson 1967	0.55		2.3	0.3	0.05	3.2±1.0	—
Howell & Shakeshaft 1966	1.3±0.2	≦0.1	2.2±0.2	0.5±0.2	—	2.8±0.6	2
Penzias & Wilson 1965, Penzias 1968	0.8±0.4	≦0.1	2.3±0.3	<0.2	0.05	3.3±1.0	3
Roll & Wilkinson 1966	1.08±0.15	—	3.0±0.2	<0.0015	3.8±0.2	3.0±0.5	—
Stokes et al. 1967	0.08±0.06	<0.05	1.37±0.1	—	—	$2.69^{+0.16}_{-0.21}$	4
Stokes et al. 1967	0.15±0.05	<0.15	4±0.1	—	—	$2.78^{+0.12}_{-0.17}$	4
Welch et al. 1967	1.9±0.2	≦0.1	4±0.2	—	—	2.45±1.0	5
Ewing et al. 1967	0.21±0.06	0.03±0.01	4.6±0.2	—	0.5±0.1	3.09±0.26	6
Wilkinson 1967	0.12±0.04	<0.05	6.5±0.2	—	—	$2.56^{+0.17}_{-0.22}$	4
Puzanov et al. 1968	—	—	17.0	—	—	3.7±1.0	5
Kislyakov et al. 1971	5±0.4	—	14.7±1.2	—	—	2.4±0.7	—
Boynton et al. 1968	0.21±0.12	—	11.5±0.22	—	—	$2.46^{+0.40}_{-0.44}$	4
Millea et al. 1971	0.21±0.11	≦0.02	11.8±0.22 12.1± ~0.4	—	—	2.61±0.25	—
Boynton & Stokes 1974	—	—	1.21±0.37	—	—	$2.48^{+0.50}_{-0.54}$ $\langle T \rangle = 2.74 \pm 0.087$ K normalized $\chi^2 = 0.44$ 14 degrees of freedom	7

See overleaf for footnotes.

FOOTNOTES FOR TABLE 1

[a] Atmospheric radiation entries are typical numbers for a data set.

[b] Notes:

1. The data analysis assumed that the cosmic background has a Rayleigh-Jeans spectrum and that the galactic component can be characterized by a power law spectrum. The two points together produce one measurement of the background temperature and the magnitude of the galactic emission.
2. Atmospheric contribution is calculated from other data, not measured in the course of the experiment.
3. Penzias & Wilson (1965) is the discovery observation. Penzias (1968) gives a corrected value for the measured temperature.
4. The four Princeton experiments, due to their small error bars, have the largest weight in determining the average temperature. Looking at the data from the four experiments together, one can see that the measured contribution of the emission by the reflector scales only marginally with the square root of the frequency. The emissivity of idealized metal surfaces in the case $E_{rf} \perp$ to the plane of incidence varies as $\varepsilon \sim 2 \cos\theta\sqrt{\nu/\sigma}$ where θ is the angle of incidence, ν the rf frequency, and σ the conductivity (cgs units). An aluminium reflector at 290 K has a minimum theoretical emission of 0.09, 0.125, 0.170, 0.27 K_{ant} at 3.2, 1.58, 0.856, and 0.33 cm for $\theta = 30°$.
5. The published result has been converted to thermodynamic temperature.
6. The emission by the horn antenna in this experiment is the estimated difference between the radiative contributions of two similar horns, one pointed to the load, the other to the sky. The published result has been corrected for an error in the way atmospheric absorption enters the measurement of the background radiation.
7. The only 3 mm experiment in which the atmospheric contribution is less than the cosmic background. The apparatus was not calibrated using a primary calibration source during the airborne measurements. It was calibrated before and after flight. The properties of the calibrator were not remeasured and assumed to be the same as in Boynton et al. (1968).

$\Delta P = KTB$. It becomes convenient to measure power in terms of a temperature. Measurements of the background radiation and liquid helium reference sources at wavelengths shorter than 3 cm show substantial deviations from the Rayleigh-Jeans spectrum; the power is not proportional to the thermodynamic temperature. To relate the received power to the calibration, it is useful to define the concept of an antenna temperature, T_{ant}. The temperature of a Rayleigh-Jeans source that radiates the same power as the actual source at a thermodynamic temperature T and frequency f:

$$kT_{ant} = hf/e^{hf/kT} - 1. \tag{3}$$

The general practice has been to measure all terms in units of antenna temperature and then to convert the CBR contribution to a thermodynamic temperature. Several of the references have not been consistent in this regard and the results in Table 1 have been adjusted accordingly.

(*b*) *Antenna*

The antenna design in background experiments is critical. The background radiation was discovered by Penzias & Wilson (1965) primarily because a very low side-lobe antenna had been constructed at Bell Laboratories for satellite communications. It is most unlikely that any general purpose radio antenna existing at that time could have been used to make the discovery with any degree of confidence. The remaining observations in Table 1 were carried out with special purpose horn antennae.

Since the background radiation covers the entire sky, there is no optimum antenna beam size to investigate the spectrum unless one wants to avoid discrete local sources. Most of the spectrum experiments have used beam widths large by radio astronomy standards, 4° to 20°, but still small enough to allow zenith angle scanning to measure the atmospheric emission. The primary concerns are antenna thermal emission and the reduction of antenna diffraction at large angles to the optic axis—the side lobes. The importance of controlling the side lobes is shown by a simple calculation. Let the main beam, observing the CBR at 3 K, include a solid angle of 0.02 steradians (10° beam). The 300 K earth, airplane, or spacecraft fills the 2π steradian backplane. If the contribution from the backplane is to be less than 10% of the CBR, the point source response of the antenna for angles greater than 90° to the optic axis must be less than 10^{-6} (−60 db) of that along the optic axis, and still smaller if the experiment is to measure the spectrum at high frequencies where the Rayleigh-Jeans approximation for the CBR is no longer valid. Since the off-axis response of the antenna is usually a steep function of the angle from the optic axis, the contribution from atmospheric emission, determined by scanning the zenith angle, can be confused by an increase in the ground radiation contribution from poorly suppressed side lobes.

Most of the antennas used in the low frequency experiments were single mode rectangular or cylindrical horns 10 to 15 wavelengths wide at their last diffracting surface. The field distribution at the horn mouth is close to cosinusoidal giving a far field angular response function at best varying as $\sim(2n \sin \theta)^{-4}$ at large angles where n is the aperture width in units of the wavelength and θ the angle to the optic axis. These horns were just barely good enough and most groups resorted to placing large metallic reflectors under and around the horn to reflect the "cold" sky into the antenna back lobes.

The high precision experiments pioneered by the Princeton group used a horn aimed at a mirror as the antenna. In this scheme the radiometer was held fixed throughout the experiment while the mirror was rotated to perform zenith scanning or removed for calibration. This technique eliminated a possible systematic error source arising from changes in the radiometer offset due to varying gravitational loading of the waveguide plumbing. However, the mirror is an additional polarization- and angle-sensitive emitting surface in the beam.

In the past few years substantial advances in low side-lobe horn designs have been made. The narrow-band corrugated horns used in the U2 experiment to measure the large angular scale anisotropy of the CBR (Gorenstein et al. 1978) have demonstrated a back-lobe rejection of 10^{-8} (−80 db) (Janssen et al. 1979). Flared broad-band multimode (apodizing) horns developed for balloon-borne spectrum measurements (Mather 1974,

Woody 1975) have been designed with the Keller theory of geometric diffraction (Levy & Keller 1959, Mather 1980). The flared horns, tested at JPL, also exhibit back-lobe rejection of 10^{-8} or smaller (Janssen & Weiss 1977).

The thermal emission by the antenna is not a serious problem at low frequencies and is measured by varying the temperature of the antenna while looking into a cold load or at the sky. In those experiments where the calibrator covered the entire antenna aperture, antenna emission does not enter the accounting procedure in first order. High frequency observations are more troubled by antenna emission both because the emissivity of the metal surfaces grows at least as fast as the square root of the frequency and because the CBR power is not rising as fast as a Rayleigh-Jeans spectrum. The best recourse here is to cool the antenna.

(*c*) *Calibration*

The basis of absolute receiver calibration is the blackbody law; it is the only radiation source that is calculable in actual practice. The implicit assumption is that an isothermal enclosure that does not reflect or become transparent radiates a blackbody spectrum. There are a host of problems in making a practical calibrator approach the idealized limit and furthermore, given a good calibrator, in being assured that the act of placing the calibrator at the radiometer input does not affect the performance of the receiver or alter the geometry at the input in an incalculable way. The calibrator should appear to the radiometer as similar to the measured source as possible.

Most of the low frequency and all the high frequency experiments have used cryogenic reference bodies to reduce the demands on receiver linearity and to minimize the change in operating point of the square law detector when switching between the calibrator and the sky. The temperature–vapor pressure relation of liquid helium is known to better than 0.1% and with reasonable care cryogenic thermometry can be performed reliably to this precision. The calibrators are constructed by terminating a waveguide or light pipe on a prismatic or conical absorber several wavelengths thick that is in good thermal contact with the cryogen. The termination is designed to trap the radiation through multiple reflections by the poorly reflecting absorber material. The central difficulty in the calibrator designs has been the thermal gradients at the transition from the cryogenic environment to the warm world outside, the problems being emission by the warmer sections of the waveguide and from windows used to avoid condensation of air in the liquid helium. These contributions are not negligible; in some experiments, in fact, they are comparable with the emission by the absorber. As the frequency increases this problem becomes more acute.

The emissivity of the calibrator is determined by reflection measurements, using $\varepsilon = 1 - R$, and is generally larger than 99% for narrow-band calibrators. Broad-band calibrators are more difficult to design. The reflectivity of the calibrator has to be known because, in use, emission by the warm receiver components (i.e. waveguides, local oscillators, horns) is reflected by the calibrator back into the receiver and this effect is not balanced out when the receiver looks into the sky.

Most of the detailed considerations involved with the interaction of the calibrator, receiver, and the thermal gradients are eliminated if the entire apparatus is maintained at cryogenic temperatures. This has been the practice in high frequency measurements and is clearly indicated for any new precision measurements at lower frequencies.

(*d*) *Atmospheric Emission and Absorption*

The profound role of the atmosphere in the measurements of the CBR is demonstrated in Figure 2 which shows the average atmospheric emission at four altitudes—0, 4, 14, 44 km—as well as the Planck spectra of 300, 3, and

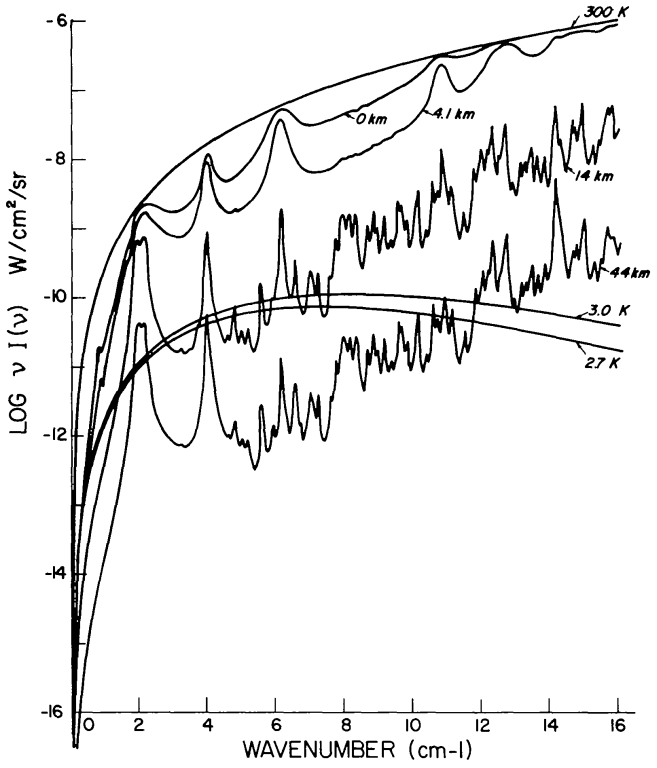

Figure 2 Zenith atmospheric emission at various altitudes drawn for an instrument with 0.04 cm^{-1} hwhm resolution. The parameters are: 0 km (H_2O, 3.7×10^{22} mol/cm^2, 300 K; O_2, 5×10^{24}, 300; O_3, 9×10^{18}, 220); 4.2 km (7×10^{21}, 250; 3×10^{24}, 250; 9×10^{18}, 220); 14 km (3.8×10^{19}, 215; 6.7×10^{23}, 215; 8×10^{18}, 215); and 44 km (2.7×10^{17}, 260; 1×10^{23}, 260; 1.7×10^{17}, 260).

2.7 K blackbodies for reference. The curves correspond to the emission observed from the ground on a good day or night (column density of 1 cm precipitable H_2O), a mountain site (2 mm), the typical altitude attained by available and instrumented jet aircraft (10μ), and balloons (0.05μ).

The atmospheric emission in this spectral region is due to the rich spectra of O_2, H_2O, and O_3. The contribution of aerosols, the other minor molecular constituents of the atmosphere, CO, N_2O, free radicals such as OH in the upper atmosphere, which emit in this spectral region, are assumed to be negligible. On the ground and mountain sites the O_2 and H_2O contributions are so overwhelming that O_3 radiation is never considered. However, at airplane and balloon altitudes this is no longer the case.

O_2 is assumed to be uniformly mixed in the atmosphere making up 23.14% of the atmospheric mass up to at least 60 km (proof positive of the uniform mixing hypothesis is missing but meteorologists argue it can't be any other way). H_2O column densities, as everyone knows, are highly variable up to altitudes of 14 km. The stratospheric concentration is a few parts per million by mass although this wasn't known until high altitude balloon experiments to measure the CBR were begun in the late 1960s. (Prior sampling experiments had measured much larger concentrations but were evidently measuring the water brought up in the apparatus.) O_3, again parts per million by mass, is concentrated in the lower stratosphere at about 30 km. The O_3 densities vary with season and latitude.

All of the emission lines come from rotational or fine structure transitions in the ground electronic and vibrational states of these molecules. The O_2 lines arise from two mechanisms—a cluster of lines at 2 cm^{-1} and a single one at 4 cm^{-1} originate from magnetic dipole transitions associated with the reorientation of the electronic angular momentum (2 Bohr magnetons from the unpaired electron spins) relative to the molecular rotation ($\Delta J = \pm 1$, $\Delta K = 0$). These lines have been extensively studied experimentally (Meeks & Lilley 1963, Liebe et al. 1977). The other lines, occurring in triplets spaced 2 cm^{-1} apart at 14, 25, 37...cm^{-1}, are magnetic dipole rotational transitions ($\Delta J = \pm 1$, $\Delta K = \pm 2$) predicted by Tinkham & Strandberg (1955a,b) and discovered by Gebbie et al. (1969). These lines play an important role in the recent and most precise measurement of the background spectrum at high frequencies (Woody & Richards 1979) and will be discussed in more detail later.

H_2O and O_3 are both asymmetric rotors with complicated spectra. H_2O, owing to its large electric dipole moment and relatively small partition sum at atmospheric temperature, is responsible for the bulk of the atmospheric emissivity in the spectral region (Benedict 1976). The influential H_2O lines are well separated in frequency. O_3, on the other hand, has a multitude of

weak lines, no less than 300 in the 1 to 20 cm^{-1} band (Gora 1959). A much appreciated and used resource is the Air Force Cambridge Geophysical Laboratory compilation of atmospheric line parameters (McClatchey 1979, Rothman 1978), which is available on magnetic tape. The compilation gives the frequency, line strength, energy of the ground state, and pressure-broadening coefficient of all known atmospheric lines from the radio through optical region.

It is well worth reviewing the assumptions and outlining the steps involved in calculating the models for atmospheric emission and absorption that have been used in CBR observations [Goody (1964) is a useful reference]. The end result of the calculation is the absorption and emission integrated over the atmospheric column at each frequency. The input parameters of a complete model would include 1. the temperature and partial pressure of the constituents as a function of altitude, 2. the individual molecular line strengths as a function of temperature, 3. the line shapes at different pressures and temperatures. To be complete, the Zeeman effect in the earth's magnetic field should be considered, especially at high altitude where the lines are narrow. The Zeeman effect makes the atmospheric propagation anisotropic. The calculation is carried out layer by layer beginning at some maximum altitude above which the radiation is deemed negligible. Each layer contributes its radiation and absorbs some fraction of the radiation from the preceding layer. The integration is continued to the altitude of the observation.

The complete calculation would pose a substantial computing problem, especially in maintaining sufficient frequency resolution to resolve the narrow lines at high altitudes. More important, the calculation is not worth doing because many of the input parameters are poorly known. Except possibly for O_2, the partial pressure of the constituents as a function of altitude is the most uncertain element. The actual temperature distribution with altitude at the time of the measurement would be the next important unknown. Furthermore, the line profiles do not conform in detail to simple theoretical models because the collisional line-broadening mechanisms depend on the colliding species and their kinetic energies. At present the only reliable way to determine the line-broadening parameters is to measure them directly with high resolution instruments.

All this is not to say the atmosphere is impossible to model but rather to urge caution in the interpretation of absolute CBR measurements where the atmospheric contribution is large.

In those parts of the atmospheric spectrum where the total absorption is small, less than $\sim 10\%$, the atmospheric emission can be measured by zenith angle scanning, since the emission is linearly proportional to the total column density of emitters. The result depends only on the assumptions of a

laminar atmosphere and homogeneity within each layer and not on the specific model. Temperature, pressure, and constituent inhomogeneities occur and in fact are the largest source of random noise in the ground-based experiments. However, they do not contribute systematic errors unless the particular observing site is anisotropic in a gross manner—because of a large lake or the ocean in the direction of the zenith scan, for example. The atmospheric and CBR contributions are separable in this case without further measurements or modeling. The total emittance B as a function of zenith angle θ is given by

$$B_{\text{total}}(f,\theta) = \alpha(f,\theta)B(f,T_{\text{atm}}) + [1-\alpha(f,\theta)]B(f,T_{\text{CBR}}) \quad (4)$$

where $\alpha(f,\theta)$ is the atmospheric absorption coefficient (in this case also the emissivity) at frequency f which is proportional to the column density of emitters (absorbers) and therefore depends on $\sec\theta$. $B(f,T)$ is the blackbody emittance at the thermodynamic temperature T. Measurement of $B(f,\theta)$ at two angles gives $B(f,T_{\text{CBR}})$ to a theoretical precision of order α^2. The procedure implied by Equation (4) has been used in all of the low frequency ground-based measurements.

Since the atmosphere at low frequencies appears primarily as a random noise source rather than a systematic one, there is hope for improved measurements of the CBR at low frequencies from the ground. The strategy of using two frequencies, X (3 cm) and K band (1.5 cm), simultaneously with up-to-date low noise radiometers, would allow measurement of the atmospheric fluctuations during the course of zenith scanning. Furthermore, rapid zenith scanning with co-addition of scans would overcome some of the dominating low frequency components of the atmospheric fluctuations.

Once self-absorption becomes important, atmospheric modeling is inevitable; Equation (4) then looks more like

$$B(f,\theta) = [1-e^{-\alpha(f,\theta,h)}]B[f,T_{\text{atm}}(h)] + e^{-\alpha(f,\theta,h)}\,B(f,T_{\text{CBR}}), \quad (5)$$

although this equation still does not represent the complete integration required.

The atmospheric absorption coefficient and the atmospheric blackbody emittance no longer appear as a simple product and must be calculated or determined separately as a function of altitude, h. Zenith scanning no longer gives a model-independent measure of the atmospheric contribution. The CBR observations at high frequency from balloons had to face up to this.

The multifilter MIT (Muehlner & Weiss 1973a,b) and the Berkeley spectrometer experiments (Woody et al. 1975, Woody 1975, Woody & Richards 1979) have used similar strategies to handle the atmospheric

contribution. At high altitudes the individual molecular lines are narrower than the spectrometer or filter resolution widths. Pressure line-broadening parameters range around 0.1–0.3 cm^{-1} per atmosphere pressure so that, at an altitude of 44 km (pressure 2×10^{-3} atm), the line widths at the base of the column are $\sim 10^{-4}$ cm^{-1}. Doppler widths are typically a factor of 10 smaller (as a consequence, absorption of the CBR is neglected). The difference between Van Vleck–Weisskopf and Lorentzian line shapes becomes negligible for such narrow lines and the Lorentzian profile is adopted for ease of calculation. All the emitting constituents are assumed to be uniformly mixed with an exponentially decreasing density as a function of altitude. The emitting column is furthermore assumed to be isothermal with the temperature measured at its base.

Under these assumptions, the power in a line from the column, integrated over all frequencies, can be cast in an analytic form that depends on the *total column density*, the line strength, the pressure-broadening parameter, and the temperature (Goody 1964). The equivalent emission width of the line is given by

$$A(\mathrm{cm}^{-1}) = 2\sqrt{\pi}\ \Delta\nu(T, P_0)\,\Gamma(x+1/2)/\Gamma(x), \tag{6}$$

where x is a dimensionless parameter indicating the degree of saturation of the line given by

$$x = S(T)\sigma/2\pi\ \Delta\nu(T, P_0). \tag{7}$$

$S(T)$ is the line strength in units of cm^{-1}/molecule/cm^2 and includes the matrix elements, multiplicity, fraction of molecules in the lower state, and the relative population difference of the two levels involved in the transition. $\Delta\nu(T, P_0)$ is the pressure-broadened Lorentzian line width at the base of the column, and σ is the column density in molecules/cm^2. The total emittance due to the line is

$$B(\nu) = B(\nu, T_{\mathrm{atm}})A. \tag{8}$$

The limiting cases are

$$A = \begin{cases} S(T)\sigma & x \ll 1 \quad \text{unsaturated lines} \\ (2s(T)\ \Delta\nu(T)\sigma)^{1/2} & x \gg 1 \quad \text{saturated lines} \end{cases}$$

When the lines are unsaturated (the emissivity at line center is much less than 1), the emission is linearly proportional to the column density and therefore the atmospheric contribution could be measured directly with zenith scanning in an almost model-independent determination. On the other hand, if the line is saturated, the emission is proportional to the square root of the column density—this is due to the assumed Lorentzian line function—and depends on the pressure-broadened line width. The increase

in emission with column density can only come from molecules emitting in the wings of the line. Zenith scanning would produce an atmospheric signal proportional to $(\sec \theta)^{1/2}$ and, providing that all lines falling into the instrument resolution width were saturated, could be used to aid in determining the atmospheric contribution. The real problem comes with a mixture of both saturated and unsaturated lines or partially saturated lines, which is the situation in the stratosphere; the O_2 lines are partially saturated, the strong H_2O lines are fully saturated, and all O_3 lines are unsaturated. Zenith scanning, with an instrument of low frequency resolution, can without knowledge of the individual constituent column densities only offer a model-independent lower limit to the atmospheric radiation and hence an upper limit to the CBR. This was the case with the MIT experiments (Muehlner & Weiss 1973a). A subsequent flight by this group (Muehlner & Weiss 1973b) used different narrow-band filters to isolate individual atmospheric lines of H_2O and a cluster of O_3 lines to determine the constituent column densities, but the signal to noise and flight duration were insufficient to improve substantially on their prior results. The spectrometer observations have enough resolution to isolate the lines of O_2 and H_2O and line clusters of O_3 so that it becomes possible, using the model outlines above, to solve for the individual column densities by fitting the observed spectrum.

A question that keeps recurring when the high frequency balloon measurements are discussed is the validity of the simple atmospheric model, which is inadequate at lower altitudes. In preparing this review I made a comparison over a restricted frequency band (10–20 cm^{-1}) of the model described above at 43 km with a 10 layered one that 1. used Doppler lines in the upper stratosphere and Van Vleck–Weisskopf lines at lower altitudes, 2. removed the isothermal restriction using the average atmospheric temperature profile with altitude (US 1966), 3. retained the uniform mixing hypothesis. The same line parameters were used in both calculations but the estimated temperature dependences of both the line strengths and line-broadening parameters were included. The result was that for the same column base temperature and pressure and equal column densities, the two models differed by less than 5%, not a remarkable result since the major emission occurs within a scale height. The difference between models is no worse than the "noise" of the uncertainties in the line parameter listings, which I estimate to be at least 10%.

Another recurring worry is the possibility that there exist *influential* atmospheric constituents that emit in this spectral region but are not now included in the line listings. The response is an equivocal "no." Finally, the notion of calibrating a CBR experiment using the atmospheric emission is a bad one; more on this later.

(e) *Galactic Background Contribution*

The next "atmosphere" is the solar system and the galaxy, the "molecules" being the astrophysical phenomena distinguished by their spectra and identified by their anisotropic distribution. The individual "molecules" are not indistinguishable and can only be characterized in a statistical sense. As a consequence, the success in modeling the "local" astrophysical background depends heavily on sampling much of the sky with extended spectral coverage.

Figure 3 shows the present best estimates of known astrophysical sources that emit in the frequency range important to CBR measurements. The CBR lies predominantly in a clear region of the local astrophysical spectrum embraced by synchrotron emission of cosmic ray electrons moving in galactic magnetic fields and free-free thermal emission by ionized gas surrounding hot stars (H II regions) at low frequencies and by the thermal emission of interstellar dust at high frequencies.

Full sky maps of synchrotron emission have been made at low frequencies, 200 MHz (Droge & Priester 1956) and 404 MHz (Pauliny-Toth & Shakeshaft 1962), where it is the major source of the galactic background and pervades the sky. There is no region of the sky which emits less than $\sim 5\%$ of the strongest sources contained in the galactic plane in a band $b \pm 10°$, $l \pm 40°$. The spectral index n, defined by $I(\nu) \propto \nu^{-n}$, ranges between 0.8 to 0.9 (Witebsky 1978) as determined by high frequency measurements in selected regions of the sky. The spectral index depends on the energy distribution of the radiating electrons and may well be different in discrete sources such as supernova remnants and in the general galactic background. In clearer regions, toward the galactic poles, the antenna temperature due to synchrotron emission is approximated by

$$T_{\rm syn} \sim 1.5 f(\text{GHz})^{-2.9} \text{ K}.$$

Strong H II regions lie primarily in the galactic plane although the Orion nebula is a notable exception. A compilation of emission by H II regions at 5 GHz is given by Lang (1978), from data of Reifenstein et al. (1970) and Wilson et al. (1970). A proper estimate of the contribution from discrete H II source emission requires knowledge of the specific H II regions in the observing beam. Typical parameters for the stronger H II regions are electron temperatures ~ 7000 K, emission measure, $N_e^2 d$, $\sim 10^6$ electron^2 $\times$ parsec per cm^6, and angular size, θ_S, $\sim 0.1°$. In the spectral region of interest to CBR measurements, 1 GHz $< f <$ 1000 GHz, quantum effects are negligible, and the optical depth in the source is much less than unity. The spectrum is almost flat, modified only by the classical Gaunt factor, giving a spectral index of approximately 0.1. The antenna tempera-

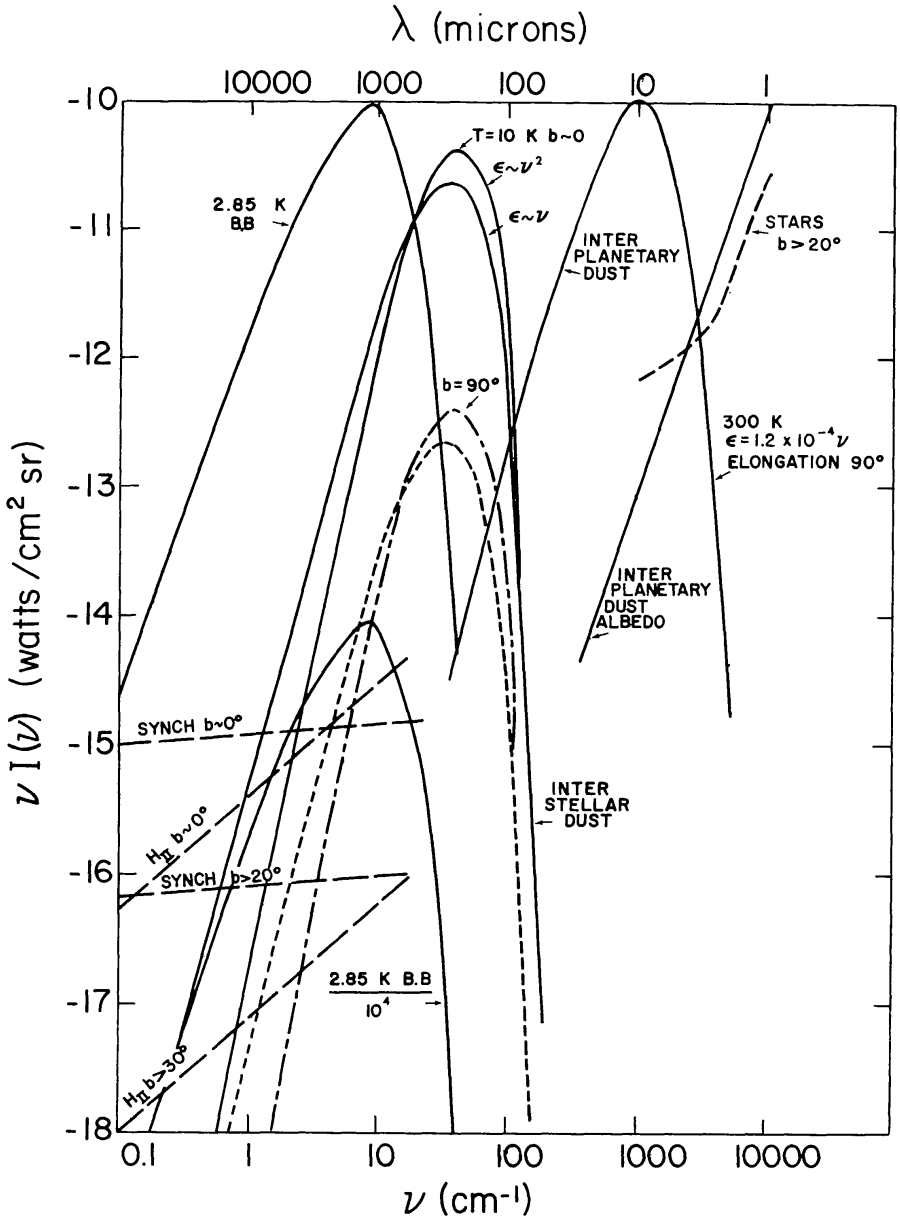

Figure 3 The astrophysical background.

ture of such a typical H II region, when diluted in a beam of angular size $\theta_B \sim 10°$, is given by (Lang 1978)

$$T_{H\,II} \sim (\theta_s/\theta_B)^2 8.2 \times 10^{-2} T_e(\mathrm{K})^{-0.35} \nu(\mathrm{GHz})^{-2.1} N_e^2 d \sim 0.4\nu(\mathrm{GHz})^{-2.1}\ \mathrm{K}. \quad (9)$$

In addition to the discrete H II regions, Hirabayashi (1974) has observed a diffuse galactic background ascribed to free-free emission with an emission measure of 4000 pc cm^{-6} and an average electron temperature of 3000 K, directly in the galactic plane. Combining this observation with the model proposed by Ellis & Hamilton (1966), which assumes the ionized

hydrogen is distributed uniformly ($N_e \sim 0.2\ \mathrm{cm}^{-3}$) in a disk 300 pc thick on either side of the plane, gives the following estimated antenna temperature (Smoot 1977) using Equation (9):

$$T_{\mathrm{H\,II}} \sim 0.07\nu(\mathrm{GHz})^{-2.1}/\sin b\ \mathrm{K} \text{ for } b > 5\ \mathrm{K}.$$

The estimates for thermal emission by interstellar dust grains shown in Figure 3 are merely suggestive since both the physical properties of the dust grains as well as the dust distribution throughout the Galaxy are still poorly known. Direct measurements of interstellar dust emission in the far infrared, $\nu < 50\ \mathrm{cm}^{-1}$, have been made solely in regions of strong emission such as in surveys of the galactic plane—at $50\ \mathrm{cm}^{-1}$ (Low et al. 1977), at 20 and $10\ \mathrm{cm}^{-1}$ (Owens et al. 1979)—and observations toward the galactic center at $28\ \mathrm{cm}^{-1}$ (Gezari et al. 1973 and Rieke et al. 1973), and at $18\ \mathrm{cm}^{-1}$ (Hildebrand et al. 1978). It has proved difficult to determine the spectrum by comparing measurements of the same objects made by instruments using different beam widths and spatial chopping techniques because many of the dusty regions are complex with both compact and diffuse emitting regions.

For $\nu \leqq 50\ \mathrm{cm}^{-1}$, the radiating efficiency of the grains is small since the wavelength is much larger than the grain dimensions, assumed 10^{-5} cm and smaller, so that even for the densest regions of the Galaxy the optical depth at $\nu < 50\ \mathrm{cm}^{-1}$ is less than 1. The emittance of a dust column is then

$$B(\nu) \sim \pi a^2 N_{\mathrm{D}} Q_{\mathrm{abs}}(\nu) B(\nu, T_{\mathrm{D}}) \tag{10}$$

where πa^2 is a typical cross sectional area of the grain, N_{B} the column density of grains, $B(\nu, T_{\mathrm{D}})$ the blackbody emittance at the dust temperature T_{D}, and $Q_{\mathrm{abs}}(\nu)$ the emissivity per grain.

The most general form of the emissivity per grain is

$$Q_{\mathrm{abs}} = a\nu f(\nu) \tag{11}$$

where $f(\nu)$ is a function of the imaginary part of the grain dielectric constant. The observations in strongly emitting regions indicate that $f(\nu)$ varies as $\nu^{0.5}$ to ν^2 and implies that the far infrared emission is most likely due to the low frequency tails of solid state absorption bands in the grains (Aannestad 1975).

Combining Equations 10 and 11, the dust brightness is proportional to the volume of dust and therefore to the mass column density. The dust brightness alone, however, cannot give the grain emissivities because the mass column density is not known directly. In lieu of a dust model, estimates of the dust mass column densities are made from the observed correlation of dust with neutral gas. The dust column densities, estimated by optical extinction and reddening, related to H I column densities determined from 21 cm line profiles (see for example Knapp & Kerr 1974) indicate that the dust-to-hydrogen mass ratio is of the order of 1%.

In the past few years observation of CO emission in dusty regions, where it is a minor constituent, have provided estimates of the H_2 densities, the major constituent. These measurements again give dust-to-neutral-gas ratios of $\sim 1\%$ (Scoville & Solomon 1975) and furthermore yield independent measurements of the dust temperature.

Along the galactic plane $|l| < 50°$, plausible parameters that fit the measured emission are $T_D \sim 25$ K, dust mass column density 3×10^{-4} gm/cm^2, corresponding to 2×10^{22} gas atoms/cm^2, individual grain emissivity $2 \times 10^{-7}\, \nu(\text{cm}^{-1})^2$, $a = 10^{-5}$ cm, and a grain density of 2 gm/cm^3. These are the parameters used in estimating the emission at $b = 0$ in Figure 3 in a beam width of 16°, the galactic plane filling about 1/15 of the beam.[2]

The estimates of dust emission out of the plane, especially toward the galactic poles, are even more uncertain. The steps involved in the estimate are the following: the dust type is assumed to be the same out of the plane as in the plane, the temperature of the dust is calculated on the basis of radiative equilibrium with the absorption of star light $T_D \sim 10$ K, the dust mass column density is estimated from H I column densities, and extinction and reddening data (Heiles & Jenkins 1976, Daltabuit & Meyer 1972). Various methods of calculating the dust mass density toward the galactic poles do not agree. Reddening data of Feltz (1972) gives an extinction due to dust of 0.000 ± 0.006 mag while Appenzeller (1975) infers an extinction $\geqq 0.03$ from stellar polarization due to dust grain alignment. The assumed ratio of gas density to visual extinction is 1.6×10^{21} atoms/cm^2/mag or $\sim 2.5 \times 10^{-5}$ gm dust/cm^2/mag so that the dust column density to the galactic poles from extinction data is close to zero or larger than 7.5×10^{-7} gm/cm^2 (4×10^{19} atoms/cm^2), while H column densities are measured directly as $1\text{–}2 \times 10^{20}$ atoms/cm^2. The dust mass column density adopted for Figure 3 is 8×10^{-7} gm/cm^2, at $b = 90°$, and to the same precision as any of these estimates, may follow a cosecant law with galactic latitude.

(*f*) *Summary of the Low Frequency Measurements*

The terms in the account have been discussed and are assembled in the following two equations. To first order in small quantities, the antenna

[2] The dust model isn't totally crazy; using simple Lorentz-Lorenz theory with one resonance, the emissivity per grain is $(2/3\pi)(\rho/m_a)(ar_e)(\nu^2 \Delta\nu/\nu_0^4)$ where m_a is the mass per atom, assuming each atom contributes one oscillator, r_e the Thomson radius of the electron, and ν_0 the resonance frequency in cm^{-1} with width $\Delta\nu$. Assuming $\Delta\nu \sim 1/10\nu_0$, $\nu_0 \sim 1000$ cm^{-1}, typical of silicates and carbonates, the emissivity/grain is of the same order of magnitude as used above.

temperature of the reference is

$$T_{\rm ref} = \varepsilon_{\rm W} T_{\rm W} + (1 - R_{\rm W})[\varepsilon_{\rm P} T_{\rm P} + \varepsilon_{\rm L} T_{\rm L}(1 - \varepsilon_{\rm P})] + R_{\rm cal} T_{\rm rec} \quad (12)$$

where $\varepsilon_{\rm W}$, $R_{\rm W}$, $T_{\rm W}$ are the emissivity, reflectivity, and temperature of the window, $\varepsilon_{\rm P}$, $T_{\rm P}$ the emissivity and temperature of the warm parts of the calibrator, $\varepsilon_{\rm L}$, $T_{\rm L}$ the emissivity and antenna temperature of the load and $R_{\rm cal}$ is the reflectivity of the reference taken as a whole. $T_{\rm rec}$ is an equivalent temperature of the receiver and antenna viewed as an emitter. The terms, when known, are listed in Table 1 for the various experiments.

The antenna temperature, looking at the sky, is

$$T_{\rm sky} = (1 - \varepsilon_{\rm ant})[\varepsilon_{\rm atm}(\theta) T_{\rm atm} + f_{\rm ant}(\theta) \varepsilon_{\rm grd} T_{\rm grd} + (T_{\rm Gal} + T_{\rm CBR})(1 - \varepsilon_{\rm atm}(\theta)] + \varepsilon_{\rm ant} T_{\rm ant}, \quad (13)$$

where $\varepsilon_{\rm ant}$ and $T_{\rm ant}$ are the emissivity and temperature of the antenna, $\varepsilon_{\rm atm}(\theta)$ and $T_{\rm atm}$ are the emissivity as a function of elevation angle and temperature of the atmosphere, $f_{\rm ant}(\theta)$ is the side-lobe response of the antenna at the ground with emissivity and temperature, $\varepsilon_{\rm grd}$ and $T_{\rm grd}$, $T_{\rm Gal}$ is the antenna temperature of the Galaxy, and finally $T_{\rm CBR}$ the antenna temperature of the cosmic background radiation. Equations (12) and (13) apply broadly to all the experiments. However, the analysis of any particular experiment may require modifications of the two equations. For example, if the reference is placed at the input of the antenna, Equation (12) would be multiplied by $(1 - \varepsilon_{\rm ant})$ and the emission of the antenna, $\varepsilon_{\rm ant} T_{\rm ant}$, would have to be added.

Table 1 is intended to show the magnitudes and uncertainties of the individual terms. As can be seen from the table many of the systematic error sources could be substantially reduced by operating the entire input end of the receiver and calibrator at cryogenic temperatures. The atmosphere, although a dominant random noise source, can be handled as indicated before. There is therefore a future in performing improved observations of the spectrum at frequencies 1 to 90 GHz from the ground.

(*g*) *High Frequency Observations of the Spectrum*

The high frequency experiments have gone through two generations. The first were the rocket- and balloon-borne observations using cryogenic broad-band radiometers which laid the technological groundwork for the second and present generation of high resolution cryogenic spectrometer observations. Some of the broad-band experiments were discussed in the Thaddeus (1972) review and the final results of these observations are listed in Table 2. The earliest experiments in the late 1960s were attended by controversy; the first rocket observations of the Cornell group showed a large energy excess at high frequencies, while the first multifilter radiometer

Table 2 Summary of broad-band high frequency observations: final results

Reference	Band (cm^{-1})	Altitude (km)	Beam size (deg.)	P (side lobe + warm parts) / P (total)	P (atmosphere) / P (total)	CBR (K thermodynamic)
Houck et al. 1972	7.7–25	144	~2	?	—	$\leqq 4.1$
Williamson et al. 1973	1.7–12.5				—	$3.4^{+1.4}_{-3.4}$
	1.7–16.7	325	20	?	—	$5.1^{+0.8}_{-1.5}$
	1.7–33.3				—	$3.8^{+0.8}_{-1.9}$
Muehlner & Weiss 1973a,b	1–5.4	44, 39	10	<0.04	0.13	$2.7^{+0.4}_{-0.6}$
	1–7.8			<0.04	0.09	2.8 ± 0.2
	1–11.1			<0.05	$\geqq 0.53$	$\leqq 2.7$
	1–18.5			<0.02	$\geqq 0.73$	$\leqq 3.4$
Dall'oglio et al. 1976	7.1–11.1	3.5	2	?	$\geqq 0.8$	$\leqq 2.7$

balloon experiments of the MIT group showed an excess in one of three spectral channels. By the early 1970s the rocket experiments, in particular those of the Los Alamos group and a new set of balloon observations of the MIT group using 5 spectral channels, settled the controversy. Furthermore, with the improved understanding of the atmospheric emission by 1973, the balloon experiments had established that there was a peak in the CBR spectrum and that the total power was consistent with the extrapolation of the ground-based low frequency measurements. The detailed shape of the spectrum was, however, not measured.

Some of the underlying problems in the early experiments are still manifested in the second generation experiments. The worst and unavoidable problem is just the fact that a fussy absolute observation must be carried out by remote control; the effect of this is that in the course of the experiment what might have been an easy calibration or test for a systematic error, or iteration in the experiment design, turns into a substantial and often expensive engineering project. The next order difficulty is due to interaction of three factors: small observation times, inadequate test facilities, and low sensitivity detectors. The nonthermal equilibrium environment—a 3 K sky, a hot earth below, and in the case of a balloon experiment, a warm and condensable atmosphere surrounding the apparatus—are difficult to simulate in terrestrial test facilities. As a consequence the final testing for systematic errors and in principle the calibration under the actual observing conditions must (or should) be carried out during the course of the experiment. The total observing time in a rocket observation is measured in minutes while for balloons it is approximately 10 hours. At very high altitudes where the atmospheric emission is smallest, the stratospheric winds are irregular and strong and the observing times may only be a few hours. With time so limited, a premium is put on having sensitive detectors to test for systematic error sources such as the contribution from warm parts of the surroundings and side-lobe response, to mention just two. The detectors have improved considerably. In the early experiments the detector noise equivalent power (NEP) was $\sim 10^{-11}$ to 10^{-12} W/Hz$^{1/2}$, just barely good enough to measure the total power in the CBR in seconds of integration time with systems of 10% optical efficiency and an étendue of 0.1–0.3 cm^2 sr. Present day detectors (composite bolometers) are a factor of 100 to 1000 more sensitive and the second generation experiments have made good use of them. But the fact remains that a table, such as Table 1, developed for the low frequency experiments, cannot be assembled for the high frequency experiments under observing conditions, and further, *none* of the high frequency experiments have experienced a primary calibration during flight.

All the high frequency spectroscopic observations of the CBR have employed Fourier transform spectrometers—Michelson interferometers. In these devices the incident radiation is split between two paths and recombined after one path is delayed relative to the other. The output signal as a function of the delay is the autocorrelation function of the radiation which, Fourier-transformed, becomes the power spectrum.

Fourier transform spectrometers are the logical choice for measuring the small power in the CBR with present day detector technology since they offer a wide spectral range, typically 2 decades, multiplexed on one or two detectors, and a large étendue, 0.1 to 0.5 cm^2 sr. The optical efficiency of the spectrometer in the millimeter and sub-millimeter range can approach 100% by using polarizing Michelson interferometers (Martin & Puplett 1969) in which the beam division is performed by a polarizer, an almost ideal optical component at these wavelengths. The frequency resolution is adjustable and limited by the maximum delay for which beam divergence or wave front distortion and displacement within the instrument destroys the relative spatial coherence of the two recombined paths. Resolutions of a few tenths of a wavenumber are typical for the instruments that have been used.

Fourier transform spectroscopy is not without hazards, the most serious being the opportunities for frequency distortion of the measured spectrum. Total intensity variations due either to fluctuations in the input signal (random noise) or incurred by the scanning (systematic errors), transform into spurious frequency components in the spectrum. Systematic spectrum distortions can also result from periodic errors in the mechanism that produces the delay. Careful design reduces these errors and thorough calibration can uncover them. A safe way to reduce their effect is to limit the optical bandwidth of the system but this of course limits the spectral coverage. The high optical efficiency, étendue, and multiplexed frequency coverage also put burdens on the detector linearity. Consequently calibration of the spectrometer requires care so as not to saturate the detector and is best carried out with cryogenic thermal sources.

The emittance measurable with a Fourier transform spectrometer is given qualitatively by

$$B_{\text{input}}(\nu) - B_0(\nu) = (\text{S/N})(\text{NEP})/\varepsilon_{\text{opt}}\, T(\nu) A\Omega\, \Delta\nu_{\text{res}} t^{1/2} \qquad (14)$$

where $T(\nu)$, $A\Omega$, and ε_{opt} are the overall optical transfer function, étendue, and optical efficiency of the system t is the total observing time using a detector with a given NEP to achieve a signal to noise S/N, in estimating the emittance in a frequency resolution element $\Delta\nu_{\text{res}}$. $B_0(\nu)$ is the thermal radiation by the interferometer enclosure or an absorbing surface entering the other port of the interferometer or incident on the detector during the alternate half of the chopping cycle when the instrument "looks" at itself. The contribution from this term produces an offset which, if constant

throughout the measurement, can be determined from the external absolute calibration.

The design of the three high frequency spectroscopic instruments used in CBR measurements are shown in Figures 4, 5, and 6. The Queen Mary College balloon-borne instrument (Beckman & Robson 1972, Beckman et al. 1974, Robson et al. 1974), Figure 4, is a cryogenic polarizing Michelson interferometer operated at 1.4 K at 40 km altitude. The instrument parameters are 0.1 cm^2 sr étendue, 0.25 cm^{-1} unapodized resolution, 6° beam width maintained at a 50° zenith angle during flight. The beam was defined by the 45° off-axis paraboloid collimator at the entrance of the interferometer section after the beam had traversed a warm 50μ polyethlyne window (not shown in the figure) and a stationary entrance polarizer followed by a rotating polarizer used as a chopper. Two InSb hot electron bolometers detect the beams reflected and transmitted by the output polarizer yielding two interferograms 180° out of phase. The technique of chopping with a rotating polarizer eliminates the signal that is not modulated by the delay and thereby reduces one opportunity for frequency distortion of the spectrum. The overall system transfer function has not

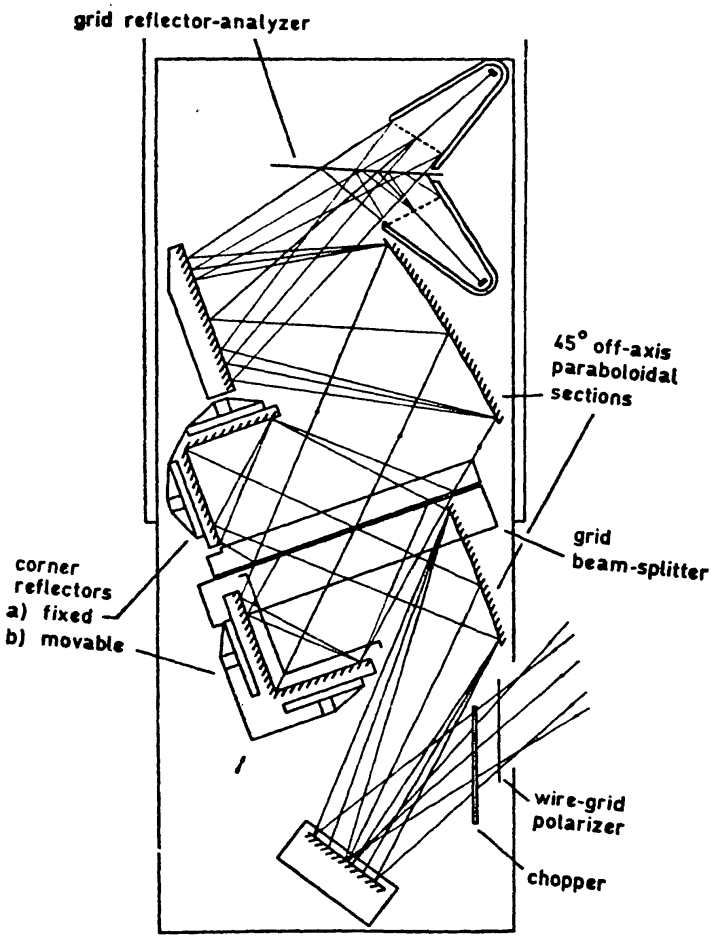

Figure 4 The Queen Mary College polarizing Michelson Interferometer.

been published but must be dominated by the high frequency roll off of the InSb detectors beginning near 10 cm^{-1} varying as $1/\nu$ and then further attenuated above 40 cm^{-1} by the reduced efficiency of the polarizers as the wavelength approaches the polarizer grid spacing (100μ).

I have difficulty in evaluating the results of the experiment, Figure 7, as there are inconsistencies in the data and the accounting of the radiation incident on the instrument is incomplete. The emission by the warm polyethlyne window, which is not removed during the observation, is unknown and may never be known as it is possible that frost condensed on it. An estimate of the atmosphere emission has not been published. However, an attempt (on my part) to model the atmosphere as observed in this experiment, especially in the critical minimum between 8 and 18 cm^{-1}, fails by a substantial margin. The contribution of the ground in the beam side lobes due to diffraction by edges at the entrance optics has not been published; finally, the calibration of the instrument in flight is not established.

The Berkeley balloon-borne experiment, Figure 5 (Mather 1974, Mather et al. 1974, Woody 1975, Woody et al. 1975, Woody & Richards 1979), has been flown twice successfully with improvements in the apparatus between

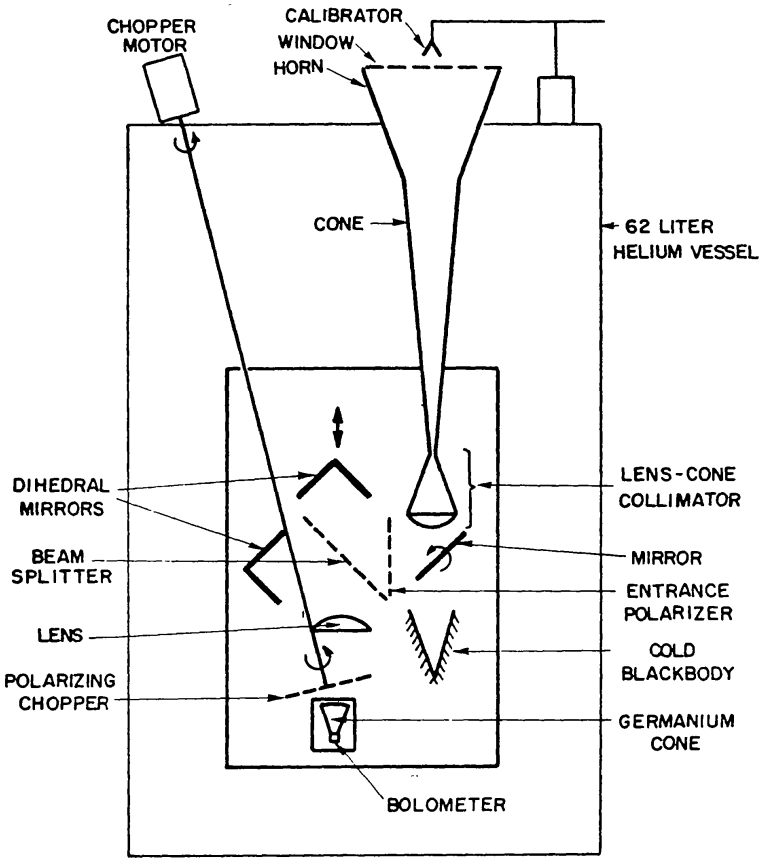

Figure 5 The Berkeley polarizing Michelson Interferometer.

flights. The instrument is again a polarizing Michelson using germanium bolometers. A composite bolometer maintained at 0.3 K (NEP $\leqq 1 \times 10^{-15}$ W/Hz$^{1/2}$) was used in the second flight, which enhanced the sensitivity of the instrument by a factor of 10. The instrument parameters are 0.23 cm^2 sr étendue, maximum unapodized resolution 0.14 cm^{-1}, 6° beam width, and an overall optical efficiency in mid-band $\sim 1\%$. A significant feature of the design is the beam-forming cone, held at liquid helium temperature, which has a demonstrated and calculable off-axis rejection of 10^6 at 60° and greater for larger angles. In the second flight an even better cone was used in concert with ground shields. Zenith scanning measurements carried out during flight demonstrated that the large angle contributions from the earth were less than $5 \times 10^{-13}\, \nu^{1/2}$ W/cm^2 sr cm^{-1}. In flight, the window over the cone was removed. The primary calibration was carried out on the ground with cryogenic calibration sources placed in the beam-forming cone. Calibration in flight, however, was estimated with an ambient temperature

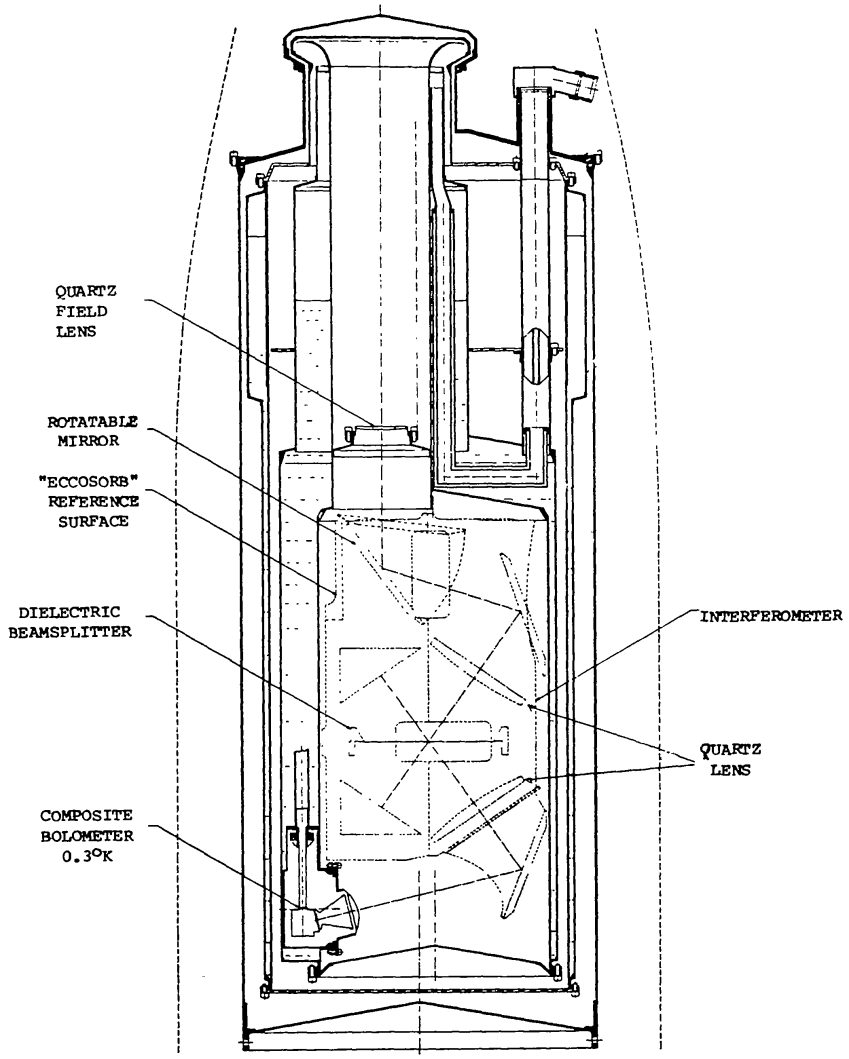

Figure 6 The rocket-borne Michelson interferometer of Gush.

secondary calibrator that could be swung into the beam. The cold blackbody source inside the interferometer at the temperature of the interferometer enclosure served to establish the offset.

The data of the second flight, Figure 8, are the most precise measurements of the CBR spectrum to date at high frequencies. (The data of the first flight is much the same with decreased signal to noise.) Panel *a* is the instrument transfer function which has been rolled off at high frequencies by a low pass filter at the detector. Panel *b* is the total measured spectrum uncorrected for the instrument transfer function while *c* is the fitted atmospheric emission spectrum using the techniques described previously. The scheme used by the group was to fit the interferogram rather than the spectrum to the atmospheric model. This streamlines the computations, eliminating the need to calculate the convolution of the instrument response function with the fitted spectrum. Panels *d* and *e* are the residuum, in principle the CBR at 0.28 and 1.8 cm^{-1} resolution. The data corrected for the instrument transfer function are given in numerical form in Table 3 (D. P. Woody, 1979, private communication).

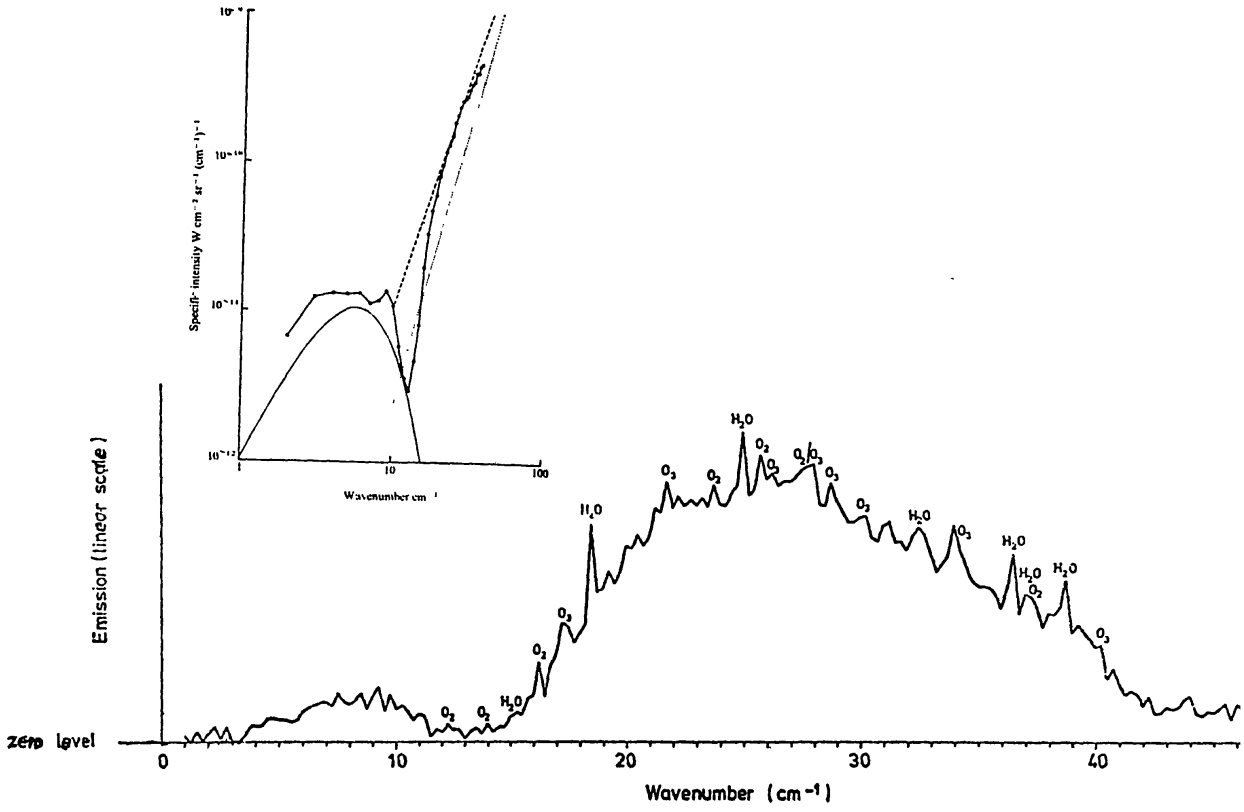

Figure 7 Spectra of the sky derived from the Queen Mary College instrument. The lower trace is the total measured spectrum including the CBR, an unknown window emission, and the atmosphere at 40 km (50° zenith angle) uncorrected for the instrument transfer function and without an absolute vertical scale. The unapodized resolution of the spectrum is 0.25 cm^{-1}. The insert is the corrected spectrum including several estimates of the window emission. The solid line is the difference between a 2.7 K and a 1.4 K spectrum.

The Berkeley data deserves close scrutiny because the major terms in the accounting are measured. Treating the errors in flux determination at each frequency as independent, the best fit to a Planck spectrum, with temperature as the only fitted parameter, is $T_{CBR} = 2.96$ K at only a 35% χ^2 contour—a 1 in 3 chance that data with the assumed random errors would fit as poorly as it does if the true spectrum were thermal at this temperature. In other words, the deviations from a thermal spectrum at 2.96 K are statistically significant. The question is, are these deviations real or artifacts of observation? Caution driven by experience dictates that we be hard on the experiment. The weakest link in all the high frequency CBR spectrum experiments is in the absolute calibration, not so much in the spectral

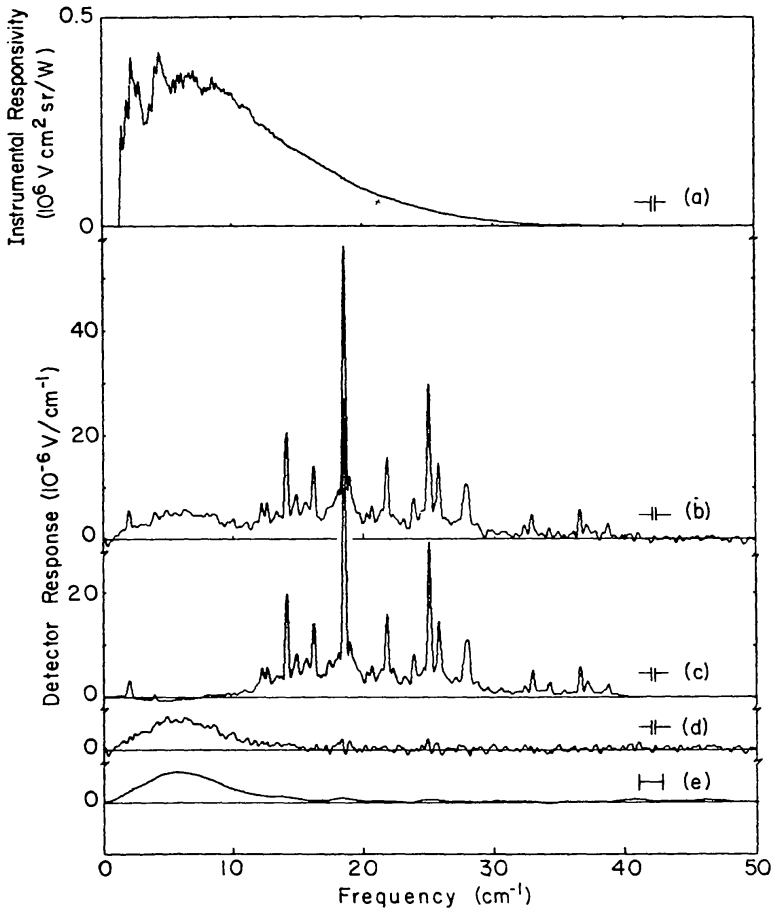

Figure 8 The Berkeley spectrum. Panel *a* shows the instrument transfer function. Panel *b* shows the total measured spectrum uncorrected for the instrument transfer function. The spectra are derived from asymmetric interferograms of 3.72 and 0.48 cm optical delay on either side of the central maximum. The apodization used is $(1-x^2/L^2)^2$. The resolution of the larger optical delay is 0.28 cm^{-1} but with wings from the shorter delay. Panel *c* is the best fit of *b* to the model atmosphere and instrument offset. Panel *d* shows the residual and *e* the same residual with 1.8 cm^{-1} resolution. The lines at 12, 14, and 16 cm^{-1} are a group of the O_2 pure rotational lines discussed in the text.

Table 3 Tabular results of the Berkeley experiments (D. P. Woody, 1979, private communication)

ν (cm^{-1})	Average flux (10^{-12} w/cm^2 sr cm^{-1})	1σ flux limits		1σ T_{CBR} limits (K)	
		min.	max.	min.	max.
2.38	8.74	7.76	9.99	3.05	3.57
3.40	12.13	11.02	13.67	2.95	3.29
4.41	14.81	13.65	16.51	2.97	3.22
5.42	16.05	14.81	17.89	2.97	3.18
6.44	16.09	14.86	17.94	2.98	3.16
7.45	13.89	12.76	15.57	2.91	3.07
8.46	12.42	11.36	13.98	2.92	3.07
9.48	8.63	7.71	9.89	2.79	2.94
10.49	6.64	5.21	7.75	2.76	2.91
11.50	5.52	4.48	6.74	2.75	2.95
12.52	4.07	2.69	5.47	2.66	2.97
13.53	4.92	2.82	7.15	2.80	3.23
15.20	1.87	—	4.10	—	3.15
17.28	0.96	—	3.07	—	3.27
20.03	0.70	—	1.81	—	3.36
22.89	0.48	—	5.76	—	4.21

response of the instrument but rather in the overall frequency-independent scale factor that converts the measured signal into an absolute power incident on the instrument.

In the Berkeley experiment, primary calibration before and after flight agreed but the instrument was not directly calibrated with the same precision during flight, the properties of the secondary ambient temperature calibrator not being well enough known. If one then assumes (without specific justification) that the instrument behaved differently in flight, one might try a two-parameter fit to the data, fitting to a thermal spectrum and a frequency-independent overall calibration factor. The results of this procedure are $T = 2.79$ and a calibration factor of 1.27. The χ^2 contour is close to 90%, a very good fit. Woody & Richards (1979) point out this fact and argue that a 27% calibration error is inconsistent with the emission measured by the atmospheric O_2 lines. The argument hinges on the fact that emission by O_2 is the one atmospheric contribution that can be calculated directly. The calculation is built on the following assumptions: 1. the O_2 column density (uniformly mixed) is given by the barometric pressure at altitude, 2. the column temperature distribution is known, 3. the line shapes are known, and finally 4. the tabulated line parameters are correct.

In preparing this review I redid the O_2 calculations independently and

agree with the Woody & Richards result using the current best theoretical estimates of the line strengths and line widths of the magnetic dipole rotational transitions ($\Delta K = \pm 2$) (Greenebaum 1975, Liebe et al. 1977, Weiss 1980). However, there is little direct experimental evidence of the line strengths, and in particular the pressure widths, except for measurements of insufficient absolute precision by Gebbie et al. (1969), which incidentally give smaller line strength than the theoretical values. Furthermore, the Zeeman effect of O_2 in the earth's magnetic field must be treated in detail and this is still in progress. The O_2 fine structure line, $\Delta K = 0$, at 4 cm^{-1} is far better known and would serve as a more reliable calibration but the instrument transfer function is changing rapidly at this frequency. The conclusion is that there are too many uncertainties in the calculation to allow an *absolute* calibration to a precision of 30% using the atmospheric emission.

The rocket-borne instrument of Gush (1979), Figure 6, performed the first spectrometer observations of the CBR above the atmosphere. The observations took place in the approximately 7 minutes while the payload was between 370 and 150 km altitude. The instrument is a conventional but cryogenically cooled Michelson interferometer using a dielectric pellicle beam splitter and a composite bolometer operated at 0.3 K. The interferogram is developed by varying the delay at a constant rate without additional beam chopping (rapid scan mode of operation). The instrument transfer function is determined by the reflection spectrum of the beam splitter at long wavelengths, becoming more inefficient the longer the wavelength, and by both the beam splitter and the high audio frequency roll-off of the detector and associated electronics at short wavelengths. The optical bandwidth of the interferometrically unmodulated component of the input signal is large, extending past 35 cm^{-1}, and this may have aggravated one of the difficulties experienced in the experiment. The instrument was calibrated before and after flight with a cryogenic reference source.

Unfortunately the results of the experiment, Figure 9, are tentative because the analysis of the data requires modeling of a significant time-varying radiative contribution from the rocket clam shell covers that moved unexpectedly to the edges of the spectrometer beam. Another time-varying and significant correction had to be made for the temperature variation of the entire instrument due to venting of helium efflux gas during the course of the flight.

Figure 10 summarizes the direct measurements of the CBR spectrum and includes the determinations using the excitation temperature of CN observed in molecular clouds at 3.79 and 7.58 cm^{-1} (Thaddeus 1972, Hegyi et al. 1974, Danese & DeZotti 1977). The figure gives the thermodynamic

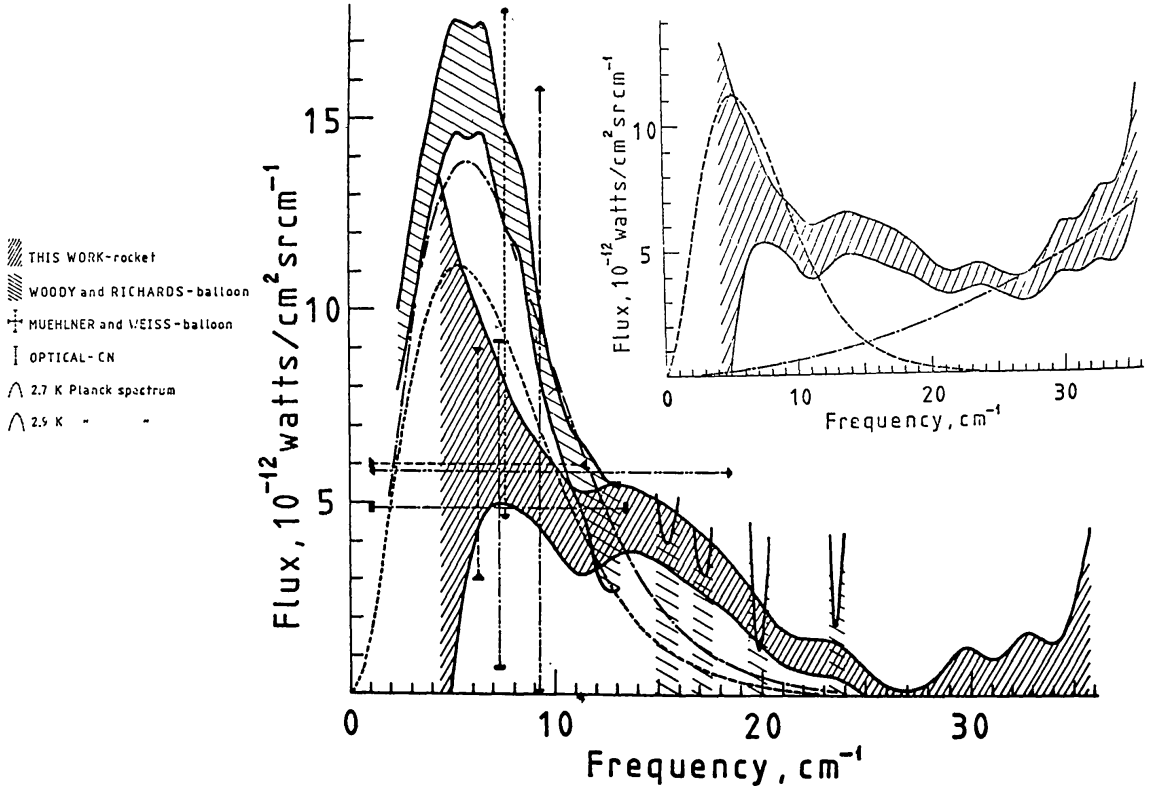

Figure 9 Rocket data of Gush. The inset shows the measured spectrum corrected for the instrument transfer function. The spectrum includes a contribution from hot objects at the edges of the beam modeled by the dot-dash line. The larger figure is a composite of various measurements of the CBR spectrum at high frequency.

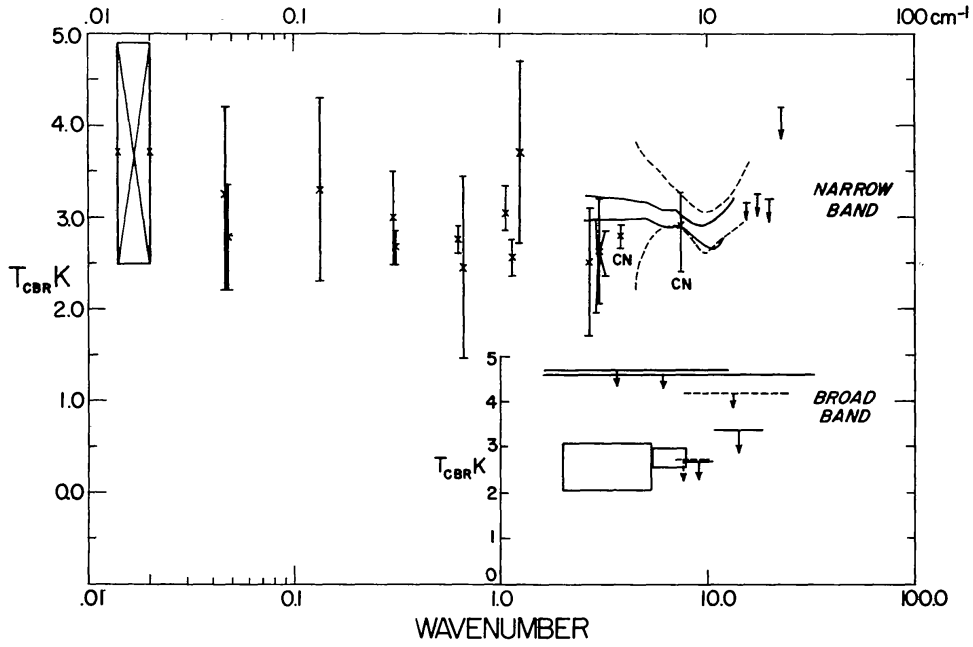

Figure 10 Summary of the measurements of the thermodynamic temperature of the CBR as a function of frequency.

temperature of a blackbody source with the same flux as that measured. The uncertainty in flux is related to the uncertainty in temperature by

$$\frac{\Delta T}{T} = \frac{x}{[\ln (1+x)](1+x)} \frac{\Delta B}{B},$$
$$x = (e^{h\nu/kT} - 1). \tag{15}$$

In summary, the overall shape of the spectrum is thermal, characterized by a single parameter, the temperature. Considering the moderate precision of the low frequency experiments and the uncertainties in the high frequency observations, it is, in my opinion, too early to fruitfully analyze the present data for the subtle distortions that may discriminate different cosmic histories. Another generation of observations is needed.

CBR measurements using optical spectroscopy to probe the state of excitation of interstellar molecules equilibrated to the background radiation have not advanced since 1974. It would be delightful to observe the CBR at different locations in the universe and at different times by in situ measurements using molecules in other galaxies. The idea may be fanciful but not entirely impossible.

MEASUREMENTS OF THE LARGE ANGULAR SCALE INTENSITY DISTRIBUTION OF THE CBR

The most convincing evidence that the background radiation is of cosmological origin—due to very distant sources if not the primeval explosion—is its isotropy, or more explicitly, that it does not share the anisotropic distribution associated with local sources such as the solar system or the Galaxy. The CBR, in fact, exhibits such a high degree of isotropy on both small ($<1°$) and large angular scales, short of the dipole term, as to pose a quandary. On small angular scales, no evidence has yet been found for granularity, thereby stringent limits are set on any discrete-source hypothesis for the origin of the background. On the other hand, at some level, still not observed, small scale anisotropies must occur as density perturbations in the early universe are believed to have preceded the presently observed aggregations. The status of these observations is not part of this review [see the article by Partridge in Ulfbeck (1980)]. On large angular scales ($\geqq 10°$), the anisotropy of the CBR is less than 1/3000, limited only by measurement uncertainties, lending strong support to the naïve assumptions of homogeneity and isotropy made in developing the spherically symmetric cosmological models, but leaving the puzzle of how unconnected regions of the universe could have evolved so identically.

In addition to the search for evidence of intrinsic cosmic anisotropies, such as might be due to aspheric expansion or large scale anisotropies in the

primeval matter distribution, an impetus for the large angular scale isotropy experiments has been the measurement of the kinematic anisotropy associated with the earth's motion relative to the distant sources of the CBR. This anisotropy had to exist at least on a level of 10^{-4} due to the earth's orbital motion around the sun in the unlikely case that the sun were at rest with respect to these sources. The anisotropy, now definitely observed at a 10^{-3} level is easily derived by a special relativistic calculation of the intensity measured by an observer moving relative to the walls of a blackbody cavity. The anisotropy retains a Planck spectrum but with an observation angle–dependent temperature (dipole term) given by

$$T(\theta) = T_0(1-v^2/c^2)^{1/2}/1-v/c\cos\theta \sim T_0(1+v/c\cos\theta), \quad v/c \ll 1,$$

where T_0 is the temperature observed in a frame at rest with respect to the sources, v is the velocity of the observer, and θ is the angle between the observing direction and the velocity.

Kinematic anisotropies of higher order (quadrupole) could exist if the universe rotates (Collins & Hawking 1973) or is filled with long wavelength gravitational radiation (Burke 1975). In general, the intensity distribution expanded in spherical harmonics is a convenient method of interrelating observation and theory in this almost spherically symmetric system. To date, no positive evidence exists for moments higher than the dipole; however, as the measurement sensitivity improves and, in particular, the sky coverage becomes more complete, interesting limits (if not measurements) can be set on the higher moments. Both extended sky and spectral coverage will become essential to unscramble the effect of local sources which are expected (Figure 3) to become important at 10^{-4} anisotropy levels even in the clearest region of the CBR spectrum. The measured spectrum of the dipole anisotropy is close to thermal. If this holds for higher order anisotropies, it becomes a discriminant against the local sources with their own characteristic spectra. Sky coverage is also required to break the correlation in estimates of the amplitude of different multipole moments. Higher order moments, if they exist, corrupt estimates of the lower order moments in fitting the multipole expansion with a data set derived from partial sky coverage.

Isotropy experiments do not have the same character as those designed to measure the CBR spectrum. The major difference is, of course, that isotropy experiments make relative measurements. The quantity measured is the difference in intensity from different directions; absolute calibration, therefore, plays a secondary role. Furthermore, because one is looking at a fixed structure in the celestial sphere, the differential data can be tested for internal consistency. Apparatus- and environment-generated anisotropies

can, in principle, be removed by observing the same celestial locations under different experimental conditions. In other words, the data alone, without further accounting as in the spectrum observations, can reveal whether or not the experiment is in trouble. The ultimate systematic errors come from local astrophysical sources, in particular from extended objects or regions of low surface brightness which may have eluded less sensitive sky surveys.

Receiver or detector sensitivity is at a premium in these experiments because the CBR anisotropies are small and tests for systematic noise in the instruments have to be carried out at the same low levels. Present day receivers at 20–30 GHz have sensitivities (Equation 1) ~ 50 mK/Hz$^{1/2}$. Observation of a systematic effect at the 10^{-3} anisotropy level requires ~ 10 minutes of integration time. In the near future, Maser preamplifiers will be used at 20 GHz, increasing the sensitivity by a factor of 10 to 20 (S. Gulkis and D. T. Wilkinson, private communication). Broadband mm and sub-mm incoherent radiometers using composite bolometers have achieved sensitivities ~ 1 mK/Hz$^{1/2}$ (2.7 K). However, at these high frequencies the galactic dust background (systematic errors) and the residual atmospheric fluctuations, even at balloon altitudes (random errors), intrude.

Table 4 presents the results and some of the characteristics of large scale anisotropy experiments. All experimets, except those of Penzias & Wilson (1965) and Wilson & Penzias (1967), who noted in their discovery paper that the background was isotropic to 10%, have been carried out by comparing the intensity from one part of the sky with that from another without reference to an absolute calibrator. The early ground-based experiments were plagued by the large galactic background at long wavelengths and atmospheric emission fluctuations at shorter wavelengths where the galactic background is smaller. In these experiments, the radiation from two directions at the same elevation angle (to equalize the average atmospheric contribution) is compared as the earth's rotation sweeps the beams over the sky. Various scanning strategies were used. Partridge & Wilkinson (1967) compared the radiation from the celestial equator with a fixed point at the celestial pole using a single beam switched by a large mirror. This experiment established that the CBR anisotropies were less than a few parts in a thousand. Conklin (1969, 1972) compared the radiation entering two horns set at 30° to the zenith (fixed declination 32°), one pointing toward the east, the other toward the west. The horns were periodically interchanged in order to search for systematic differences in the apparatus. This experiment was the first to report a 24 hour anisotropy but the result was tentative because the large galactic contribution had to be modeled by extrapolation with a poorly known spectral index from 400 MHz sky maps. The observation, which measured the East–West com-

Table 4 Results of large scale anisotropy experiments

Reference	λ (cm)	f (GHz)	ν (cm^{-1})	Altitude (km)	Receiver noise (mK/Hz$^{1/2}$)	Beam width (deg.)	$\frac{\Delta T_{rms}\ \text{mK}}{\text{Beam width}}$	ΔT mK (24 hr)
Wilson & Penzias 1967	7.35	4.08	0.14	0	—	—	<100	—
Partridge & Wilkinson 1967	3.2	9.4	0.31	0	—	10	~ 10	1 ± 2.2
Conklin 1969	3.75	8.0	0.27	3.8	65	12	—	1.6 ± 0.8 (projected $\delta = 32$)
Conklin 1972								2.3 ± 0.9 equitorial
Boughn et al. 1971	0.86	35	1.16	0	1600	4	~ 50	7.5 ± 11.6
Henry 1971	2.96	10.1	0.34	24	~ 250	15	3	3.2 ± 0.8
Corey & Wilkinson 1976 Corey 1978	1.58	19	0.63	25	100	~ 10	3	2.9 ± 0.7
Muehlner & Weiss (Muehlner 1977)			3–10	39	90	18	3	<3.3
Smoot et al. 1977 Gorenstein 1978	0.9	33	1.11	20	44	7	1.5	3.5 ± 0.6
Cheng et al. 1979	1.21	24.8	0.83	27	51	8	1.5	2.99 ± 0.34
Analysis includes Corey 1978	0.955	31.4	1.05	27	45	6	1.5	
Smoot & Lubin 1979	0.9	33	1.11	20	44	7	1 (95% CF)	3.1 ± 0.4
Muehlner & Weiss 1980	—	—	3–10	39	90	18	3	2.8 ± 0.8

Note: Since this review was written the measurement of the large scale anisotropy in the 3–20 cm^{-1} band has been reported by Fabbri et al. (1980). The data imply a dipole anisotropy of amplitude $T_D = 2.9^{+1.3}_{-0.6}$ mK in the direction $\alpha_D = 11$ h 24 m ± 40 m, $\delta_D = 3 \pm 10°$. The data require a fit to a quadrupole-like term of amplitude $0.9^{+0.4}_{-0.2}$ mK.

Table 4–*continued*

Reference	ΔT mK (24 hr galactic correction)	RA_D (hr)	δ_D	ΔT mK (12 hr)	Sky coverage
Wilson & Penzias 1967	—	—	—	—	29 Locations distributed $70° > \delta > -20°$ $2\text{ hr} < \alpha < 20\text{ hr}$
Partridge & Wilkinson 1967	—	—	—	4.9 ± 2.0	Circle, $\delta = -8°$, vs celestial pole
Conklin 1969	2.9	$13 \pm {}^{1.9}_{2.3}$			Circle, $\delta = 32°$,
Conklin 1972		11	—	—	East-West difference 60° apart
Boughn et al. 1971	—	—	—	5.5 ± 6.6	Circle, $\delta = 0°$, beam switched ± 2.1 hr RA Celestial pole reference
Henry 1971	<0.5	10.5 ± 4	-30 ± 25	—	North–South only $3\text{ hr} < \alpha < 15\text{ hr}$ $-13° < \delta < 77°$
Corey & Wilkinson 1976 Corey 1978	<0.3	12.3 ± 1.4	-21 ± 21	—	$12\text{ hr} < \alpha < 20\text{ hr}$ $-13° < \delta < 77°$
Muehlner & Weiss (Muehlner 1977)	—	—	—	—	$4\text{ hr} < \alpha < 6\text{ hr}$ $15\text{ hr} < \alpha < 23\text{ hr}$ $-13° < \delta < 77°$
Smoot et al. 1977	<0.5?	11.0 ± 0.5	6 ± 10	<1	22 spots $0\text{ hr} < \alpha < 18\text{ hr}$ $5° < \delta < 65°$
Gorenstein 1978				$Q(\alpha, \delta)$	
Cheng et al. 1979 (Analysis includes Corey 1978)	<0.3	12.3 ± 0.4	-1 ± 6	<2	$12\text{ hr} < \alpha < 26\text{ hr}$ $-13° < \delta < 77°$
Smoot & Lubin 1979	—	11.4 ± 0.4	9.6 ± 6	$Q(\alpha, \delta)$ <1 $Q(\alpha, \delta)$ $Q(\delta)$	14 spots $4\text{ hr} < \alpha < 17\text{ hr}$ $-50° < \delta < 25°$
Muehlner & Weiss 1980	<1	9.6 ± 1.5	-9 ± 20		$14\text{ hr} < \alpha < 31\text{ hr}$ $-13° < \delta < 77°$

ponent of the anisotropy, agrees with newer measurements, but it took courage to publish the result at the time. Boughn et al. (1971) attempted an isotropy measurement at 35 GHz, where the galactic contribution is small. The instrument was a differential radiometer with one beam (the reference) pointed to the zenith and the other switched periodically between two points on the celestial equator 2.1 hr either side of the meridian plane. Atmospheric emission fluctuations dominated the noise budget, partly aggravated by the experiment design, but nevertheless highlighting one of the main difficulties with ground-based large angular scale anisotropy experiments. The sensitivity to a dipole anisotropy increases as the sine of the beam separation. However, the effect of atmospheric emission fluctuations grows as well, since the fluctuations become more independent the larger the beam separation.

The definitive observations have all been carried out above the bulk of the atmospheric emission at balloon or jet airplane altitudes. The balloon-borne experiments by Henry (1971), Corey & Wilkinson (1976), Muehlner & Weiss (1977, 1980), and Cheng et al. (1979) have been similar in concept (Figure 11). The intensity in two beams 90° apart, bisected by the zenith and separated by 180° in azimuth, is differenced at a rapid rate (10–200 Hz). The beams are formed with low side-lobe horns and further protected from radiation by the ground and the lower atmosphere with a large ground shield that reflects the sky. The entire instrument is set into rotation about the zenith at about 1 revolution per minute. The rotation serves both to scan the sky and to allow measurement of the intrinsic anisotropy of the apparatus. The azimuth is determined with magnetometers using the earth's field as a reference. Provision is made to measure or eliminate the systematic noise terms that might be synchronous with the rotation. The most serious of these have been magnetic interactions in the ferrite components of the microwave receivers which perturbed the results of Henry (1971). Other effects are rotation-induced wobbles of the apparatus or pendulation of the instrument which cause an azimuth-dependent variation in elevation angle of both beams, thereby modulating the atmospheric emission. The wobbling motions are measured with tilt sensors and pendulation is determined from the magnetometers. The effect of these motions can also be determined by using a differential radiometer at a frequency where the atmospheric emission is stronger but not saturated (Muehlner 1977). Finally, although balloons follow the stratospheric winds, wind shears do occur and cause differential temperature variations in the instrument as it rotates under the balloon. These are measured with sufficient precision using differential thermometers. Typical balloon flights last 8–10 hours, the balloons traveling at almost constant declination. With the given beam configuration, about 1/4 of the sky can be covered in a single flight.

The signal is the difference in intensity measured in the two beams as a function of azimuth. The analysis is made by averaging this signal over a set of rotations occurring in the time it takes the celestial sphere to move about 1/2 a beam width. These averages are then expanded in a harmonic series in multiples of the rotation frequency. The fundamental component includes

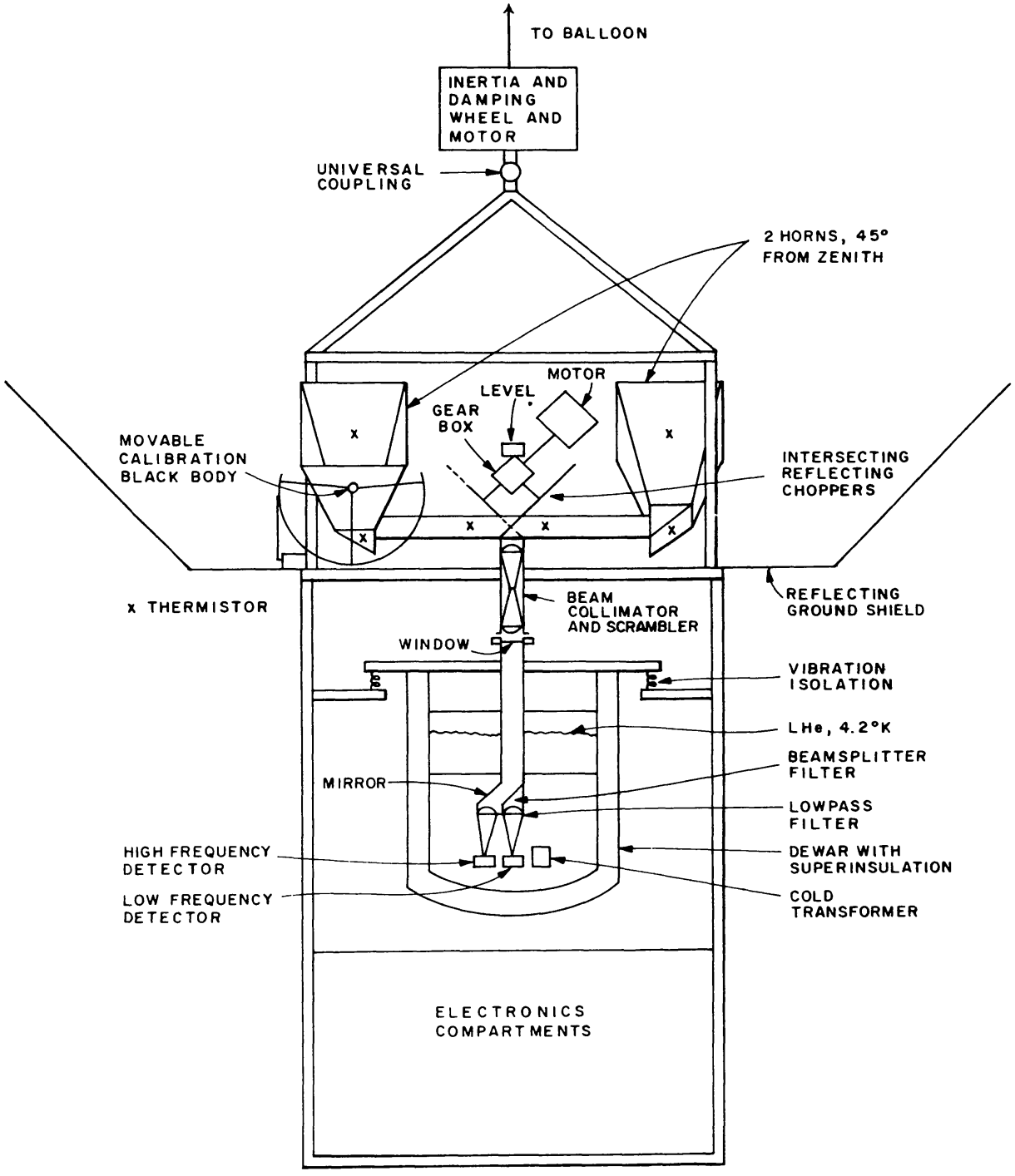

Figure 11 A typical balloon-borne large angular scale isotropy experiment. This one is the M.I.T. instrument. The more successful Princeton balloon-borne instrument is similar in concept.

information on all multipole moments of the intensity distribution; higher odd harmonics exclude the lower order anisotropy moments and are a diagnostic for discriminating discrete sources. With beams 180° apart in azimuth, the apparatus is insensitive to even harmonic components although signals at these frequencies are valuable in diagnosing internal difficulties such as radio frequency interference and microphonics.

A dipole anisotropy of amplitude T_d pointing along α_d (RA) and δ_d (dec) would produce a fundamental component with polar and equatorial projections given by

$$\Delta T_{N-S} = 2T_d \sin EA\ [\sin \delta_d \cos \delta - \cos \delta_d \sin \delta \cos (\alpha - \alpha_d)]$$
$$\Delta T_{W-E} = 2T_d \sin EA\ [\cos \delta_d \sin (\alpha - \alpha_d)], \quad (16)$$

where α and δ are the right ascension and declination of the zenith and EA is the elevation angle of the beams (45°). The best fit of Equation (16) to the data of Chang et al. (1979) is shown in Figure 12.

The balloon-borne observations were begun by Henry (1971) at 10 GHz. He measured the North–South component of the dipole anisotropy. The first definitive measurement (sufficient sky coverage and signal to noise) is that of Corey & Wilkinson (1976) at 19 GHz followed by the observation

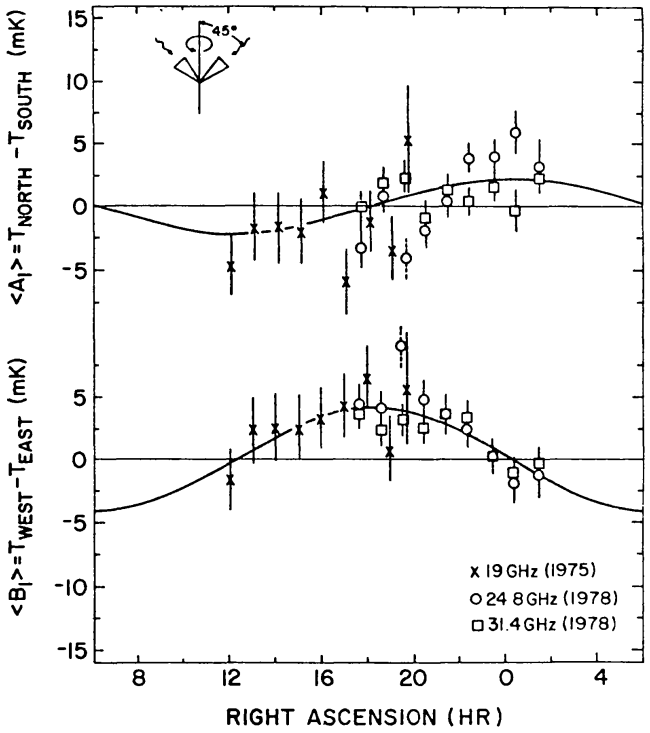

Figure 12 The Princeton anisotropy measurements using a balloon platform. The best fit to a dipole anisotropy is shown as the solid line.

using the U2 airplane (Smoot et al. 1977) to be discussed below. Isotropy measurements in the spectral band embracing the blackbody peak, 3–10 cm^{-1}, were carried out from balloons by Muehlner and Weiss (Muehlner 1977). The data, perturbed by galactic dust emission, could only be used to set an upper limit on the dipole anisotropy. With improved knowledge of the dust sources (Owens et al. 1979), the high frequency data has been reanalyzed, exhibiting a dipole anisotropy consistent with the lower frequency measurements (Muehlner & Weiss 1980). The spectrum of the dipole anisotropy appears to be close to Planckian.

The group at Berkeley (Smoot et al. 1977) has made good use of the U2 airplane as a platform to measure the large scale anisotropy. Although the airplane does not attain as high an altitude as the balloon, it offers some logistic advantages over the balloon, in particular in the relative ease of launching flights. The U2 instrument, Figure 13, is similar to the balloon-borne differential radiometers. It operates at 33 GHz and includes a 54 GHz radiometer to monitor the tilt of the airplane in the atmosphere. The radiometer beams are separated by 60° and are switched at 100 Hz. The entire apparatus is turned periodically within the airplane housing to measure intrinsic instrument anisotropies. Finally, the flights are arranged

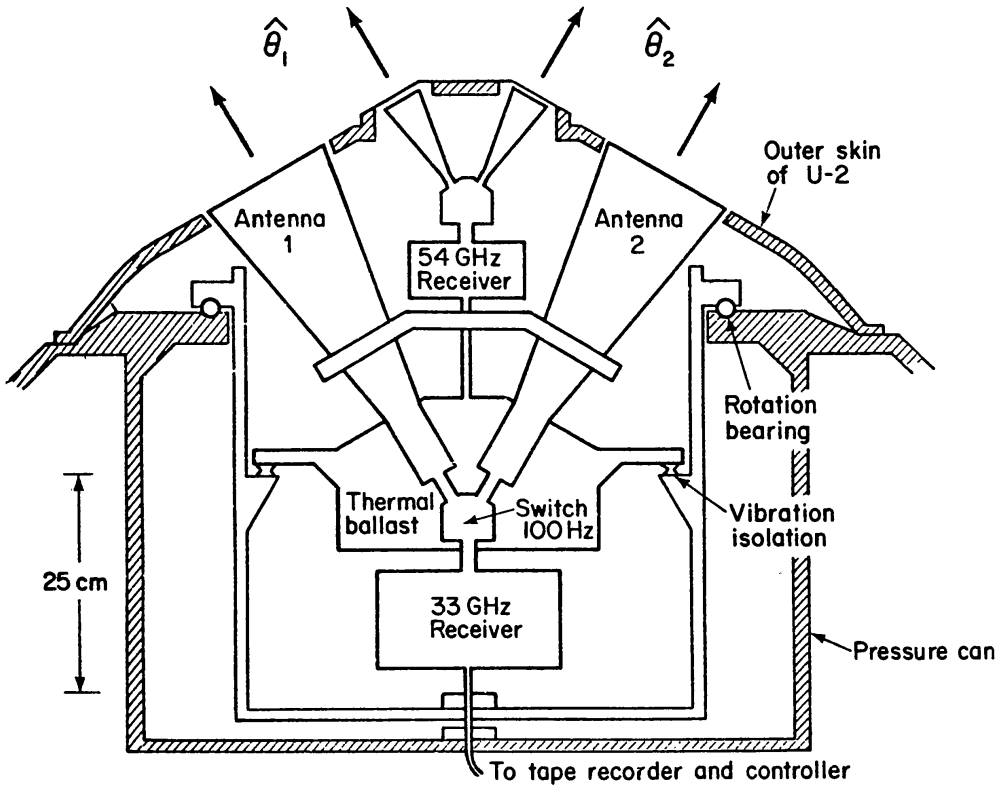

Figure 13 The U2 differential radiometer.

so as to observe the same regions of the sky with the airplane reversed in direction to account for anisotropies that might be fixed in the airplane coordinate system.

The observing and data analysis strategy (Gorenstein 1978, Gorenstein & Smoot 1980) is different than in the balloon experiments. Observation points in the sky are selected, Figure 14*b* and *d*, and the difference in intensity of the two beams is fit to a dipole distribution in a celestial coordinate system. The presentation of the data and the fit, Figure 14*a* and *c*, superposes all points that make the same polar angle with the dipole axis. Figure 14, as it stands, cannot be used to make a unique correspondence with a sky map.

With the enhanced precision and more extended sky coverage of both the U2 (Smoot & Lubin 1979) and balloon experiments (Cheng et al. 1979), limits have been set on the five independent terms of a quadrupole moment

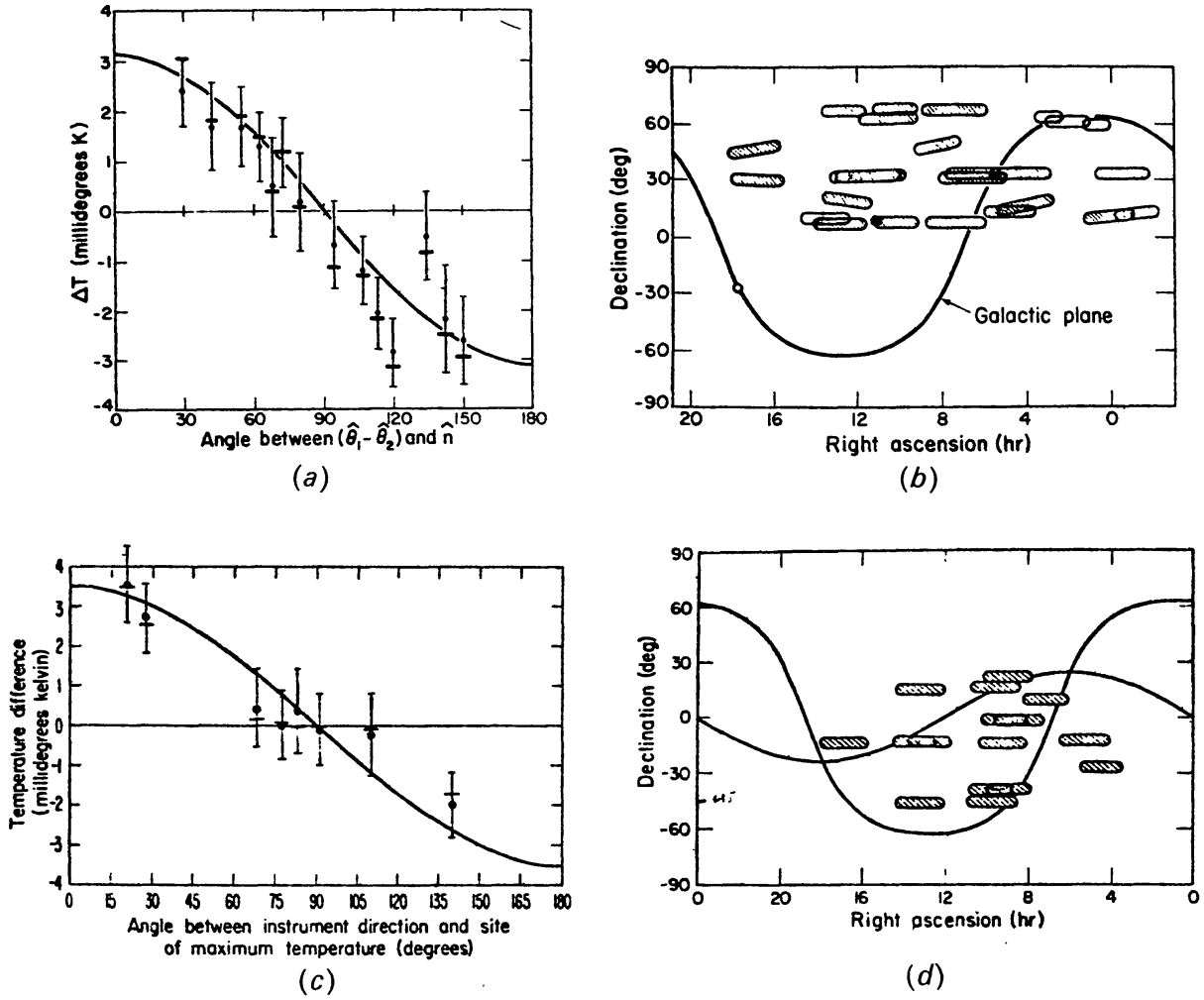

Figure 14 The Berkeley anisotropy data using the U2 airplane. Panel *a* and *c* show the fit to the same dipole anisotropy using the data derived from sky coverage shown in *b* and *d*.

Table 5 Multipole fits of Berkeley and Princeton data (Lubin & Smoot 1979, Cheng et al. 1979)

Quadrupole and dipole fit

Princeton:

$$T = \mathbf{T}\cdot\mathbf{n} + \sum_{m=-2}^{2} (a_{2m} + ib_{2m})Y_{2m}$$

Berkeley:

$$T(\alpha,\delta) = T_0 + T_x \cos\delta\cos\alpha + T_y \cos\delta \sin\alpha + T_z \sin\delta$$
$$+ Q_1(\tfrac{3}{2}\sin^2\delta - \tfrac{1}{2}) + Q_2 \sin 2\delta \cos\alpha + Q_3 \sin 2\delta \sin\alpha$$
$$+ Q_4 \cos^2\delta \cos 2\alpha + Q_5 \cos^2\delta \sin 2\alpha \qquad \alpha = \text{RA},\ \delta = \text{DEC}$$
$$Q_1 = \sqrt{5/4\pi}\,a_{20},\quad Q_2 = -\sqrt{15/8\pi}\,a_{21},\quad Q_3 = \sqrt{15/8\pi}\,b_{21},$$
$$Q_4 = \sqrt{15/8\pi}\,a_{22},\quad Q_5 = -\sqrt{15/8\pi}\,b_{22}$$

	Berkeley	Princeton
T_x(mK)	-2.78 ± 0.28	-3.27 ± 0.57
T_y	$+0.66\pm0.29$	-0.17 ± 0.73
T_z	-0.18 ± 0.39	-0.10 ± 0.72 $(T_z+1.125Q_1)$
Q_1	$+0.38\pm0.26$	—
Q_2	$+0.34\pm0.29$	$+0.22\pm0.50$
Q_3	$+0.02\pm0.24$	$+0.26\pm0.67$
Q_4	-0.11 ± 0.16	-0.05 ± 0.36
Q_5	$+0.06\pm0.20$	-0.22 ± 0.38
Dipole fit only		
T_x	-3.01 ± 0.24	-2.98 ± 0.30
T_y	$+0.39\pm0.25$	-0.24 ± 0.30
T_z	$+0.52\pm0.23$	-0.06 ± 0.31
T mK	3.1 ± 0.4	2.99 ± 0.34
$\delta°$	9.6 ± 6	-1 ± 6
α hr	11.4 ± 0.4	12.3 ± 0.4
v(2.7 K) km s^{-1}	344 ± 44	$332\ \pm38$
f(GHz)	33	19, 24.8, 31.4

of the CBR intensity distribution, Table 5. The balloon observations, all having been carried out at the same zenith declination, are not able to separate the polar dipole contribution, T_z, from the exclusively polar quadrupole term Q_1. Of the approximately 20 U2 flights that have been made, four were in the southern hemisphere specifically to break the

correlation of these terms. The maximum magnitude of the quadrupole moment is less than 1 mK.

The large scale isotropy experiments are now at a level where further progress requires instruments of increased sensitivity or the use of observing platforms allowing substantial increase in integration time. More extended sky coverage is essential.

LIMITS ON THE LINEAR POLARIZATION OF THE CBR

The degree of polarization of the CBR is another attribute that can be directly measured. Polarization anisotropies may be produced by the same sources generating intensity anisotropies and could survive if the intergalactic medium does not randomize the polarization through a dispersive Faraday rotation (Rees 1968).

Penzias & Wilson (1965) noted that over a substantial portion of the sky, the background was less than 10% linearly polarized. Nanos (1973) carried out the first systematic search for linear polarization. The instrument was a single beam X band (3.2 cm) polarization sensitive radiometer aimed at the zenith. The output signal of the radiometer was the difference in intensity of two orthogonally polarized components. By rotating the entire apparatus about the optic axis, two Stokes parameters (Q or S_1 and U or S_2) as well as the instrumental polarization asymmetries were measured. As the same beam includes both polarization states, the atmospheric fluctuations cancel in the measurement, providing only that the polarization is switched at a rate fast compared to the time scale of the atmospheric fluctuations. The observation covered a celestial circle of fixed declination, 40°, sampled every beam width, 12°, in right ascension. Each sample consists of two differences in intensity of polarization, one difference being between the North–South plane and the East–West plane and another pair at $\pm 45°$. The rms noise per point is close to receiver noise and corresponds $\leqq 0.03\%$ polarization. No statistically significant average, 24 hour or 12 hour periodic components were observed in the data at the same level of sensitivity.

A similar experiment, carried out at 9 mm ($\theta_B = 7°$) (Lubin & Smoot 1979) with increased sky coverage, $\delta = 38°$, 53°, and 63°, and a factor of about 2 improvement in sensitivity, produced a null result as well.

Caderni et al. (1978) have set upper limits on the polarization in the 3 to 20 cm^{-1} band with a balloon-borne polarimeter. The instrument consisted of a telescope with a choice of fields of view, 1/2° or 15°, coupled to a bolometer through a rotating linear polarizer. Such systems generally have intrinsic wavelength-dependent polarization anisotropies which must be

calibrated by viewing an unpolarized source with a known spectrum. The atmospheric emission, by way of the instrument polarization anisotropy, produced a large systematic polarization offset which, although measured by secant scanning, still limited the observation. The observations, extending over a patch of sky $30° \times 60°$ in the vicinity of the galactic center, set limits of $\sim 1\%$ to $\sim 0.1\%$ on the degree of polarization on angular scales of 1.5° to 40°. The limits could be improved if the experiment were done by rotating the entire apparatus rather than the polarizer as is done in the microwave experiments.

No experiments have measured the third Stokes parameter, V or S_3, to establish the degree of circular polarization of the CBR. At present all the polarization measurements are limited by instrument-derived random noise rather than by polarization anisotropies in the atmosphere or from galactic sources. It seems, therefore, that with improved instrumentation a 10 to 100 times better limit could be set before the intervention of local polarization anisotropies. The open question is on what angular scales is the search most interesting?

THE COBE PROJECT

It has long been recognized that measurements of the spectrum, especially at high frequency, and the large angular scale intensity distribution of the CBR would benefit greatly by being carried out from a long-lived space platform. Aside from the obvious and important advantages of freedom from atmospheric emission, fluctuations in the emission, and absorption, which limits the spectral range, a satellite platform offers full sky coverage with a single instrument and allows sufficient time to test for systematic errors as well as to integrate the weak CBR signals. Furthermore, a shielded apparatus in space offers a thermally controlled environment in vacuum, which facilitates absolute primary calibration with cryogenic sources.

Since 1974 a group consisting of S. Gulkis (Jet Propulsion Laboratory), M. Hauser (NASA Goddard Space Flight Center), J. Mather (NASA Goddard Space Flight Center), G. Smoot (University of California, Berkeley), R. Weiss (MIT), and D. Wilkinson (Princeton) has been involved in planning the COBE (Cosmic Background Explorer) mission. The advance possible by using a space platform should bring measurements of the CBR to the level where the dominant "noise" will be the contribution of the local astrophysical environment. The complement of instruments chosen and the mission specifications of full sky coverage with ~ 1 year lifetime are designed to discriminate the CBR from more local astrophysical sources by their spectra and anisotropic angular distribution.

The present NASA plan is to fly the COBE mission in early 1985. A

schematic diagram of the instrument is shown in Figure 15. The instrument, in sun-synchronous polar orbit, points radially out from the earth and rotates at 1 revolution per minute. A liquid helium cryostat with a 1 year storage time sits in the center of a 5 meter diameter sun and rf shield. The cryostat contains a Fourier transform spectrometer (FIRAS) and an infrared photometer (DIRBE). FIRAS (Far Infrared Absolute Spectrophotometer) points along the axis of rotation while DIRBE (diffuse infrared background experiment) points at 30° to the rotation axis. Four differential microwave radiometers (DMR) are attached to the outside of the cryostat.

FIRAS is intended to measure the CBR spectrum. It consists of a rapid-scan polarizing Michelson interferometer divided into two bands 1–20 cm^{-1} and 20–100 cm^{-1} with a minimum resolution width of 0.2 cm^{-1} at long wavelengths and a 5% resolution at short wavelengths. The beam is defined to 7° by a trumpet-shaped horn. The expected sensitivity for each field of view, in a one year mission, is $\sim 10^{-13}$ W/cm^2 sr.

DIRBE is incorporated in the COBE mission to serve two purposes: first, to measure the interstellar dust emission which may contaminate the CBR

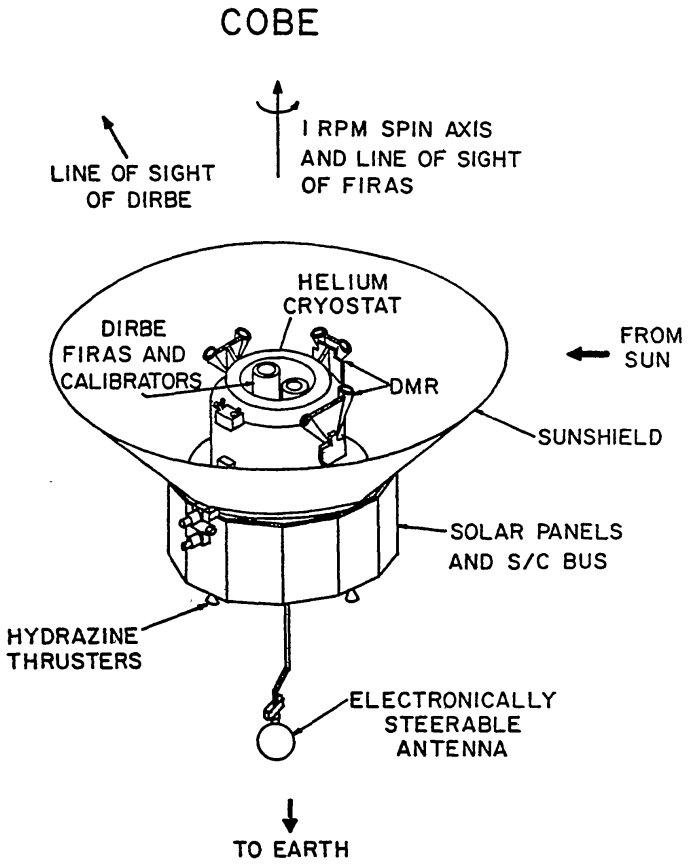

Figure 15 Schematic of the proposed COBE satellite.

spectrum at high frequencies and, second, to perform an all-sky survey of the diffuse infrared background from 1 to 250 microns which, although it is not a residue of the primeval radiation, may contain components that are the result of later epochs in cosmic history. The instrument is a multiband filter absolute photometer with a 1° field of view. The low background conditions in space and in particular in the COBE configuration should allow a sensitivity of $\sim 10^{-14}$ W/cm^2 sr per field of view in 1 year, $\lambda < 160\mu$, and about a factor of 10 worse $\lambda > 200\mu$.

The DMR experiment measures the large angular scale anisotropies of the CBR with a beam width of 7°. The differential radiometers operate at 23, 31, 53, and 90 GHz. Each radiometer compares the radiation of two patches of the sky 60° apart. The expected sensitivity in a one year mission is 0.3 mK in each of 1000 independent elements of the sky. The radiometer frequencies are chosen to measure both the CBR as well as the contamination by synchrotron and thermal emission by H II regions at low frequency and the interstellar dust at high frequencies.

The results of the COBE mission will be a set of sky maps from 1 to 10,000 cm^{-1}, which includes all the processes indicated in Figure 3, the galactic synchrotron emission, diffuse H II thermal emission, interstellar and interplanetary dust, as well as the integrated starlight. The residue will be the CBR and whatever other cosmological background might exist.

Literature Cited

Aannestad, P. A. 1975. *Ap. J.* 200:30

Alpher, R. A., Herman, R. 1975. *Proc. Am. Philos. Soc.* 119:235

Appenzeller, I. 1975. *Astron. Astrophys.* 38:313

Beckman, J. E., Robson, E. I. 1972. *Infrared Detection Techniques for Space Research*, ed. V. Manno, J. Ring, p. 63. Dordrecht: Reidel

Beckman, J. E., Clegg, P. E., Huizinga, J. S., Robson, E. I., Vickers, D. G. 1974. Paper presented at *IAU Conf., Sept. 3, 1976*, Trieste

Benedict, W. S. 1976. *Infrared Spectra of Atmospheric Molecules. AFGL-TR-76-0145*. Air Force Geophysical Lab.

Boughn, S. P., Fram, D. M., Partridge, R. B. 1971. *Astrophys. J.* 165:439

Boynton, P. E., Stokes, R. A., Wilkinson, D. T. 1968. *Phys. Rev. Lett.* 21:462

Boynton, P. E., Stokes, R. A. 1974. *Nature* 247:528

Burke, W. L. 1975. *Astrophys. J.* 196:329

Caderni, N., Fabbri, R., Melchiorri, B., Melchiorri, F., Natale, V. 1978. *Phys. Rev. D* 17:1908

Cheng, E. S., Saulson, P. R., Wilkinson, D. T., Corey, B. E. 1979. *Astrophys. J. Lett.* 232:L139

Collins, C. B., Hawking, S. W. 1973. *MNRAS* 162:307

Conklin, E. K. 1969. *Nature* 222:971

Conklin, E. K. 1972. In *External Galaxies and Quasi-stellar Objects. IAU Symp. 44*, ed. D. S. Evans, p. 518. Dordrecht: Reidel

Corey, B. E., Wilkinson, D. T. 1976. *Bull. Am. Astron. Soc.* 8:351

Corey, B. E. 1978. PhD thesis. Princeton Univ.

Dall'oglio, G., Fonti, S., Melchiorri, B., Melchiorri, F., Natale, V., Lombardini, P., Trivero, P., Sivertsen, S. 1976. *Phys. Rev. D* 13:1187

Daltabuit, E., Meyer, S. 1972. *Astron. Astrophys.* 20:415

Danese, L., DeZotti, G. 1977. *Riv. Nuovo Cimento* 7:277

Droge, F., Priester, W. 1956. *Z. Astrophys.* 40:236

Ellis, G. R. A., Hamilton, P. A. 1966. *Ap. J.* 146:78

Ewing, M. S., Burke, B. F., Staelin, D. H. 1967. *Phys. Rev. Lett.* 19:1251
Fabbri, R., Guidi, I., Melchiorri, F., Natale, V. 1980. Submitted to *Phys. Rev. Lett.*
Feltz, K. A. 1972. *Publ. Astron. Soc. Pac.* 84:497
Gebbie, H. A., Burroughs, W. J., Bird, G. R. 1969. *Proc. R. Soc. London Ser. A* 310:579
Gezari, D. Y., Joyce, R. R., Simon, M. 1973. *Ap. J. Lett.* 179:67
Goody, R. 1964. *Atmospheric Radiation.* Oxford Univ. Press
Gora, E. K. 1959. *J. Mol. Spectrosc.* 3:78
Gorenstein, M. V. 1978. PhD thesis. Univ. Calif., Berkeley
Gorenstein, M. V., Muller, R. A., Smoot, G. F., Tyson, J. A. 1978. *Rev. Sci. Instrum.* 49:440
Gorenstein, M. V., Smoot, G. F. 1980. In preparation
Greenebaum, M. 1975. *Tech. Rep. T-1-306-3-14.* Riverside Res. Inst. NY
Gush, H. P. 1979. Preprint
Hegyi, D. J., Traub, W. A., Carleton, N. P. 1974. *Astrophys. J.* 190:543
Heiles, C., Jenkins, F. B. 1976. *Astron. Astrophys.* 46:333
Henry, P. S. 1971 *Nature* 231:516
Hildebrand, R. H., Whitcomb, S. E., Winston, R., Steining, R. F., Harper, D. A., Moseley, S. H. 1978. *Ap. J. Lett.* 219:101
Hirabayashi, H. 1974. *Publ. Astron. Soc. Jpn.* 26:263
Houck, J., Soifer, B., Harwit, M., Pipher, J. L. 1972. *Ap. J. Lett.* 178:29
Howell, T. F., Shakeshaft, J. R. 1966. *Nature* 210:1318
Howell, T. F., Shakeshaft, J. R. 1967. *Nature* 216:753
Janssen, M., Weiss, R. 1977. COBE Rep.
Janssen, M. A., Bednarczyk, S. M., Gulkis, S., Marlin, H. W., Smoot, G. F. 1979. Preprint
Kislyakov, A. G., Chernyshev, V. I., Lebskii, Y. V., Mal'tsev, V. A., Serov, N. V. 1971. *Sov. Astron.* 15:29
Knapp, G. R., Kerr, F. J. 1974. *Astron. Astrophys.* 35:361
Lang, K. R. 1978. *Astrophysical Formulae.* New York: Springer
Levy, D. R., Keller, J. B. 1959. *Comments Pure Appl. Math.* 12:159
Liebe, H. J., Gimmestad, G. G., Hopponen, J. D. 1977. *IEEE Trans. Antennas Propag. AP-25*:327
Low, F. J., Kurtz, R. F., Poteet, W. M., Nishimura, T. 1977. *Ap. J. Lett.* 214:L115
Lubin, P. M., Smoot, G. F. 1979. *Phys. Rev. Lett.* 42:129
Martin, D. R., Puplett, E. 1969. *Infrared Phys.* 10:105
Mather, J. C. 1974. PhD thesis. Univ. Calif., Berkeley
Mather, J. C., Richards, P. L., Woody, D. P. 1974. *IEEE Trans. Microwave Theory Tech. MTT-22*:1046
Mather, J. C. 1980. Preprint
McClatchey, R. A. et al. 1979. *Air Force Cambridge Research Laboratory Absorption Line Parameters Compilation*
Meeks, M. L., Lilley, A. E. 1963. *J. Geophys. Res.* 68:1683
Millea, M. R., McColl, M., Pedersen, R. J., Vernon, F. L. 1971. *Phys. Rev. Lett.* 26:919
Muehlner, D. J., Weiss, R. 1973a. *Phys. Rev. D* 7:326
Muehlner, D. J., Weiss, R. 1973b. *Phys. Rev. Lett.* 30:757
Muehlner, D. J. 1977. *Infrared and Submillimeter Astronomy*, ed. G. G. Fazio. Dordrecht: Reidel
Muehlner, D. J., Weiss, R. 1980. To be published
Nanos, G. P. 1973. PhD thesis. Princeton Univ.
Owens, D. K., Muehlner, D. J., Weiss, R. 1979. *Ap. J.* 231:702
Partridge, R. B., Wilkinson, D. T. 1967. *Phys. Rev. Lett.* 18:557
Pauliny-Toth, I. I. K., Shakeshaft, J. R. 1962. MNRAS 124:61
Penzias, A. A., Wilson, R. W. 1965. *Ap. J.* 142:419
Penzias, A. A., Wilson, R. W. 1967. *Astron. J.* 72:315
Penzias, A. A. 1968. *IEEE Trans. Microwave Theory Tech. MTT-16*:608
Puzanov, V. I., Salomonovich, A. E., Stankevich, K. S. 1968. *Sov. Phys. AJ* 11:905
Rees, M. J., 1968. *Ap. J.* 153:L1
Reifenstein, E. C., Wilson, T. L., Burke, B. F., Mezger, P. G., Altenhoff, W. J. 1970. *Astron. Astrophys.* 4:357
Rieke, G. H., Harper, P. A., Low, F. J., Armstrong, K. R. 1973. *Ap. J. Lett.* 183:67
Robson, E. I., Vickers, D. G., Huizinga, J. S., Beckman, J. E., Clegg, P. E. 1974. *Nature* 251:591
Roll, P. G., Wilkinson, D. T. 1966. *Phys. Rev. Lett.* 16:405
Rothman, L. S. 1978. *Appl. Opt.* 17:3517
Scoville, N. Z., Solomon, P. M. 1975. *Ap. J. Lett.* 199:105
Smoot, G. F. 1977. *COBE Rep. No. 5002*
Smoot, G. F., Gorenstein, M. V., Muller, R. A. 1977. *Phys. Rev. Lett.* 39:898
Smoot, G. F., Lubin, P. M. 1979. *Ap. J. Lett.* 234:L83
Stokes, R. A., Partridge, R. B., Wilkinson, D. T. 1967. *Phys. Rev. Lett.* 19:1199

Sunyaev, R. A., Zel'dovich, Ya. B. 1980. *Ann. Rev. Astron. Astrophys.* 18:537
Thaddeus, P. 1972. *Ann. Rev. Astron. Astrophys.* 10:305
Tinkham, M., Strandberg, M. W. P. 1955a. *Phys. Rev.* 97:937
Tinkham, M., Strandberg, M. W. P. 1955b. *Phys. Rev.* 97:951
Ulfbeck, O., ed. 1980. *Universe at Large Red Shifts.* Proc. Niels Bohr Institut, June 24–31, 1979. *Physica Scripta* 21:599
US 1966. *U.S. Standard Atmosphere Supplements.* Washington, DC: US Gov't. Print. Off.
Weiss, R. 1980 In preparation
Welch, W. J., Keachie, S., Thornton, D. D., Wrixon, G. 1967. *Phys. Rev. Lett.* 18:1068
Wilkinson, D. T. 1967. *Phys. Rev. Lett.* 19:1195
Williamson, K. D., Blair, A. G., Catlin, L. L., Hiebert, R. D., Loyd, E. G., Romero, H. V. 1973. *Nature Phys. Sci.* 241:79
Wilson, T. L., Mezger, P. G., Gardner, F. F., Milne, D. K. 1970. *Astron. Astrophys.* 6:634
Wilson, R. W., Penzias, A. A. 1967. *Science* 156:1100
Witebsky, C. 1978. *COBE Rep. No. 5006*
Woody, D. P. 1975. PhD thesis. Univ. Calif., Berkeley
Woody, D. P., Mather, J. C., Nishioka, N. S., Richards, P. L. 1975. *Phys. Rev. Lett.* 34:1036
Woody, D. P., Richards, P. L. 1979. *Phys. Rev. Lett.* 42:925